TU
WIEN

TECHNISCHE
UNIVERSITÄT
WIEN

Master Thesis

Parameter study for 3D printing of Al5356, Al4047 and Al4043 by directed energy deposition with transferred plasma arc

performed at
Technische Universität Wien,
Institute of Chemical Technologies and Analytics
Gereidemarkt 9/164-CT
A-1060 Vienna

supervised by Ao. Prof. Dipl.-Ing. Dr.techn. Roland Haubner

by

Johannes Niedermayer, BSc.

Mat. Nr. 01025565

Hoysgasse 4a/4
A-2020 Hollabrunn
Vienna, July 2022

Affidavit

I declare in lieu of oath, that I wrote this thesis and performed the associated research myself, using only literature cited in this volume. If text passages from sources are used literally, they are marked as such. I confirm that this work is original and has not been submitted elsewhere for any examination, nor is it currently under consideration for a thesis elsewhere. I acknowledge that the submitted work will be checked electronically-technically using suitable and state-of-the-art means (plagiarism detection software). On the one hand, this ensures that the submitted work was prepared according to the high-quality standards within the applicable rules to ensure good scientific practice "Code of Conduct" at the TU Wien. On the other hand, a comparison with other student theses avoids violations of my personal copyright.

_____   _____

City and Date   *Signature*

Acknowledgement

For technical, organisational and advisory support I thank Ao. Prof. Dipl.-Ing. Dr.techn. Roland Haubner, Dipl.-Ing. Michael Kitzmantel and John Meuthen, MSc. Their expertise and their critical feedback was an essential input to this work and helped for brining it to finish.

Due an university course is not only done by writing a master thesis, but also by attending lectures, studying and doing a number of exams, I thank my dear friends and colleagues Univ.Ass. Dipl.-Ing. Dr.techn. Alexander Kirnbauer, Dipl.-Ing. Benjamin Piribauer and Thomas Waibl, BSc. for a great time with them on the technical university of Vienna but also for mastering students life.

Many thanks to my dear parents for opening me the possibility of doing an university degree - this is not a matter of course! I am honoured and humble for that I have had this privilege.

Last and most important, my thanks go to my lovely wife Carina Niedermayer, BEd, MA for supporting and encouraging me, not only during this work but also throughout the whole time on university. Thanks for your support, especially in times I did not want to hear.

Kurzfassung   Additive Fertigung (engl. additive manufacturing AM) ist eine revolutionäre Technologie, mit deren Hilfe es möglich ist Prototypen, Modelle oder Bauteile basiernd auf einem 3D-CAD Modell mit Hilfe von Fertigungsmaschinen generativ zu fertigen. Das Pontential von AM liegt vor allem in der Herstellbarkeit von geometrisch komplexen Bauteilen und in der wirtschaftlichen Anwendbarkeit für Bauteile ab Losgröße eins bis hin zu Serienbauteilen. Eine dieser AM-Technologien ist Plasma Metal Deposition (PMD) und basiert auf einem fundierten Prozess - dem Plasma Auftragsschweißen. Bei PMD werden mit einem Plasmalichtbogen und zugeführtem Draht oder Pulver, beliebige Strukturen, Schicht für Schicht aufgeschweißt, welche schlussendlich einen dreidimensionalen Körper ergeben. Diese Arbeit beschäftigt sich mit dem Einfluss von Prozessparameter, auf die mechanisch technologischen Eigenschaften von additiv gefertigten Proben aus Aluminiumlegierungen. Aus bereits vorgehenden Versuchen und Erfahrunen ist dabei bekannt, dass bei der Wahl von ungeeigneten Prozessparemter, Porosität oder Einschlüße auftreten können, welche zur Minderung der mechanischen Eingenschaften beitragen. Es soll der Einfluss der Schweißparameter auf dieses Verhalten durch zerstörende Werkstoffprüfung, vor allem mittels Zugversuch und Mikroskopie, untersucht werden. Es werden dabei die Aluminiumlegierungen AlMg5Cr (EN AW-5356), AlSi12 (EN AW-4047) und AlSi5 (EN AW-4043) behandelt und deren Eignung für die additive Fertigung mittels PMD diskutiert.

Abstract   Additive manufacturing (AM) is a revolutionary manufacturing technology, enabling to create parts, models and prototypes by a 3D-CAD model and an additive manufacturing system in a generative way. Its potential lies in the technologies character to build geometrically complex parts not achievable with any other manufacturing technology while enabling economical applications from lot size one up to series production. One of those AM-technologies is plasma metal deposition (PMD) which is based on a well established process - plasma cladding. For PMD an electric plasma arc is used to form a weld pool, by adding feedstock in form of powder or wire into the weld pool a material deposition is achieved. By moving the plasma arc and the wire along an arbitrary path, a layer is built. By stacking multiple layers over each other, a three dimensional part is finally produced. This work is about the effects of welding parameters on the mechanical properties of additive manufactured specimen made of aluminium alloys. Based on previous tests it is known that inappropriate parameters can lead to voids & pores in the material which further lead to poor mechanical properties. Therefore the influence of various welding parameters shall be analysed with destructive test procedures like tensile test and microscopy. The alloys AlMg5 (EN AW-5356), AlSi12 (EN AW-4047) and AlSi5 (EN AW-4043) will be investigated and their applicability for PMD will be discussed.

Contents

List of abbreviations and formula signs

AM	additive manufacturing
CMT	cold metal deposition
DCCP	direct current coupled polarity
DCRP	direct current reversed polarity
DCSP	direct current straight polarity
DED	directed energy deposition
EDM	electrical discharge machining
GMAW	gas metal arc welding
GTAW	gas tungsten arc welding
LCA	life cycle assessment
MMC	mixed material composites
NASA	national aeronautics and space administration
NTA	non-transferred arc
PAW	plasma arc welding
PBF	powder bed fusion
PMD	plasma metal deposition
SMD	shaped metal deposition
TA	transferred arc
UAV	unmanned aerial vehicle
UTS	ultimate tensile strength
VPPA	variable polarity plasma arc
WAAM	wire arc additive manufacturing
WFS	wire feed speed
YS	yield strength

1. Introduction

1.1 General considerations & motivation

Additive manufacturing (AM) is one of the hottest topics in prototyping, manufacturing communities and industry. The standard ISO/ASTM 52900:2021 describes additive manufacturing as the *"process of joining materials to make parts from 3D model data, usually layer upon layer, as opposed to subtractive manufacturing and formative manufacturing methodologies"* [1] - although there are already approaches to print in a volumetric way [2] which might change these definitions in future. The increasing popularity in the last 10 years of additive manufacturing is mainly credited by two events. First the expiration of the patent US5121329A of Stratasys Inc. [3] for fused deposition modelling, which enabled dozens of companies & start-ups the development of AM-systems for industrial & domestic use which triggered secondly, the massively growing AM community in both fields.

From this success also other AM-technologies participated like powder bed fusion, vat photopolymerization, material jetting or binder jetting which was a huge driver for research and development but also for their publicity. This can be seen on the growing popularity of "maker spaces", dedicated rooms or facilities in schools, universities but also in public which are equipped with a variety of manufacturing machines (mostly table-top) wherein 3D printers play an important role.

During this time another, yet not so well-known AM-technology was getting more attention - the talk is about directed energy deposition (DED). It is described as *"additive manufacturing process in which focused thermal energy is used to fuse materials by melting as they are being deposited"* [1]. While this technology strongly builds on cladding, an old and well known technology for repairing and manufacturing, it is currently rather a niche in the field of additive manufacturing. The reason for its rather low popularity mainly comes from three characteristic points. First, process based - the printed structures are what is called "near net-shape" and means

that a printed object has to be machined after the printing process to get its final shape. Second, degree of complexity - the process is limited in geometric complexity which means that internal structures, features below 1mm and lattice structures can not be printed safely. Third, application and investment - due limitation of the degree of complexity, DED is mainly dedicated for rather simple parts with dimensions ranging from 100mm up to several meters. Coming to the investment, DED turn key systems range from 200,000€ up to several million Euro - which is driven by system size, degree of automation and printing technology [4].

Although these points might suggest that there is limited use for DED on the additive manufacturing map, there are some major benefits the other AM technologies are lacking - to print on complex substrates (e.g., a shaft or bracket), to print big parts with dimensions up to several meters and to simultaneously print with multiple materials by using wire and powder feedstock. These arguments make DED an attractive technology for shipyards, mining, oil & gas, special purpose machinery and aerospace. Although DED is an emerging AM technology it is still in its infancy and many challenges like process stability, tool path planning and post processing are still in focus of R&D activities it has high potential to be part of future manufacturing methods by improving material & energy savings but also to enable production on site respectively near site to reduce transportation and logistics [5] & [6].

We also have to mention that DED and in general AM are no panacea which will generally reduce production costs or green house gases for any given part but rather are mighty technologies which can help to improve specific parts in functionality, production speed, manufacturing costs or their LCA. That said it is very unlikely that one day industry will use solely AM for manufacturing.

1.2   Aim of the diploma thesis

The aim of this work is to test three different aluminium alloys for their application with plasma metal deposition - a DED technology working with a transferred plasma arc and metal wire - and to investigate suitable process parameters in terms of creating stable mechanical properties in the printed sample parts. Further the results shall give insight to SBI GmbH into process related phenomena e.g. forming of imperfections in the metal matrix and achieved surface quality. This work also brings basics of DED technologies, service providers, system manufacturers and stakeholders as well as the principles of plasma arc welding.

2.   Literature

Additive manufacturing, rapid prototyping, 3D printing et al.

During the last 30-40 years a lot of nominations were created & rejected for generic processes. Additive Fabrication, Rapid prototyping, additive layer manufacturing, layer manufacturing, solid freeform fabrication and many more. Some of them were used as process classification, some as process designation, some as trademarks and finally some as synonym for all three of them. This chaotic use of terminology resulted in misunderstandings and an eventually abuse of registered trademarks. By introducing the ASTM committee F42 in 2009 which later started a collaboration with the ISO/TC 261, the first step for a range of standards in additive manufacturing - including terminology [1] - was set. These standards also comprised a classification of additive manufacturing technologies which can be seen in figure 2.1. While the names for the AM categories are defined by the standard ISO/ASTM 52900:2021 the further descriptions like "FUSION THROUGH" and "MATERIALS" are additions made by the author to give a short description of characteristic properties for a better understanding of the single categories.

In this work we will use the terms additive manufacturing, printing and 3D printing as comprising term for the generic build-up process of any AM-technology.

	MATERIAL JETTING	BINDER JETTING	MATERIAL EXTRUSION	POWDER BED FUSION	DIRECTED ENERGY DEPOSITION	SHEET LAMINATION	VAT PHOTO POYLMERI-SATION
FUSION THROUGH	BONDING AGENT	UV LIGHT & BINDER	HEATED PRINTHEAD	LASER BEAM; ELECTRON BEAM	ELECTRIC ARC; LASER & ELECTRON BEAM;	MICROWAVES; BONDING AGENT	UV LIGHT
MATERIALS	PLASTIC; METAL	PLASTIC; CERAMIC; METAL; SAND	PLASTIC; METAL; CERAMIC	METAL; CERAMIC; PLASTIC	METAL; MMC	METAL; PAPER; CERAMIC	PLASTIC; CERAMIC; METAL

Figure 2.1: The 7 categories of additive manufacturing according to ISO/ASTM 52900:2021. MMC = mixed material composites

2.1 History of directed energy deposition

A glimpse to the 1920s - the intellectual birth of directed energy deposition

Although the terminus *directed energy deposition* just exists since 2015, there have been technologies and approaches in the past which already fulfilled its definition (see section 2.2). The first document which comes DED closest is a patent of Mr. Ralph Baker, filed in 1920. Ralph Baker got said patent granted in 1925 which was named "*Method of making decorative articles*" (US patent nr. 1,533,300) which seems at the first glance more amusing than technically relevant. A closer look reveals the potential behind the delighting title, namely *"... to construct walls or containers by manipulating a fusible electrode helically to form superposed deposits of metal"*. The issue of electrode manipulation was not simply solved by manually manipulation but by a pantograph control, analogous to those of milling systems back in those days. Figure 2.2 shows the header of Baker´s patent, a sketch of a container made by his patented process as well as a close-up of the material layers. However, it can be said that Mr. Bakers invention was commercially not relevant and got into oblivion.
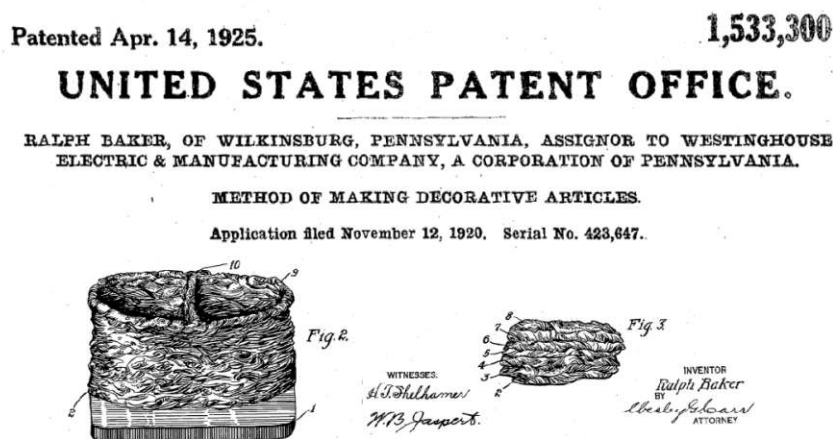
Figure 2.2: Picture of the patent of Ralph Baker; it shows a container (Fig.2) made by successively superposition of weld beads on a substrate and a close-up (Fig.3) of the build-up [7].

The development of today´s DED

Between the 1920s and nowadays, the idea of Mr. Baker was applied respectively reinvented multiple times in form of projects, feasibility studies and further patents

and often was referred as "shape welding" [8] [9].

An article of 1990 in the Journal of Nuclear Materials [10] by engineers and scientist of Siemens explains the use of shape welding for the production of elbow segments for pressure water reactors. Therefore the research team used a submerged arc welding technology and printed a half-toroid which was later cut in two pieces and further was joined by submerged arc welding and resulted in a 180° pipe elbow. In figure 2.3 the completed half-toroid can be seen on the welding machine.

Figure 2.3: 3D printed half-toroid, after printing the part was cut apart and welded together to form a 180° pipe elbow [10].

Another early user of DED was Andritz Hdyro GmbH who used the gas metal arc welding process, to additively build up pelton cups on a pre-form substrate in the early 1990´s. In figure 2.4a the substrate can be seen which consists of a casted ring with the roots of the pelton cups. 2.4b shows a close-up of the finally built-up pelton cups. This process was named "MikroGuss" which means in English "micro cast" due the cups are locally casted. According to Posch et al [11] until today about 400 pelton runners were produced by the MikroGuss technology working without any remarkable complaints. Also in the 1990´s the university of Cranfield (UK) got active in DED when they developed together with Rolls Royce a technology to print casting moulds by gas metal arc welding. They called this process *shaped metal deposition* (SMD) which later was named in wire arc additive manufacturing (WAAM) and will be treated later in this chapter.

(a)   (b)

Figure 2.4: (a) The "MikroGuss" process in action (b) Finished pelton runner "as built" [11] .

2.2 DED processes

Directed energy deposition is one of the most diverse AM-classes and is according to the ISO/ASTM 52900:2021 [1] the "*process in which focused thermal energy is used to fuse materials by melting as they are being deposited*". DED systems basically consist of a kinematic manipulation system, a controller respectively PC, a thermal energy source and a feedstock feeder. While the kinematic system is mostly either a robot or a CNC-system, the range of energy sources is much broader. Figure 2.5 shows different DED energy sources and their corresponding feedstock types, either powder, wire or both of them.
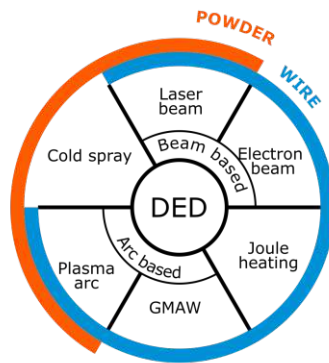
Figure 2.5: DED processes sorted by energy source and corresponding feedstock type.

Processes which can handle both material forms do have some benefits regarding material selection. Wires in generally do offer a broad range of materials, ranging from steels, aluminium, nickel-base alloys to titanium while having the benefit of lower costs than their powder counterparts which comes from the higher production costs of quality metal powders. During the last years companies like voestalpine Böhler Welding GmbH or Lincoln Electric Ltd. added special AM-metal wire to their portfolio which distinct by better surface conditions and more rigorous tolerances for the containing components.

On the other hand, the use of powder does have the advantage to get access to materials which can not be manufactured in wire form like hard metals e.g., tungsten carbide, but also gives the possibility to create small batches of alloys by mixing different components in a fast and economic way. While the GMAW based DED processes are solely using one or two wires, the plasma arc driven processes can handle both, wires and powders. The reason for this behaviour lies in the interdependency of the plasma arc power of the fed feedstock, which allows to feed wire, powder or both into the weld pool independently by the set plasma arc current. Although it is possible to feed powder into a GMAW-arc, this technology is a niche

due hard control and low process stability.

In the beam based section only the laser process can handle both material forms. The powder has to be transported to the weld pool through a hose system. To avoid clogging due e.g. bridge formation, the powder has to be pushed by a carrier gas like Argon. Due electron beam guns often work in a vacuum, this carrier gas would negatively affect the electron beam and further the AM-process.

Cold spray

At cold spray DED the used feedstock type is metallic powder which is driven by supersonic carrier gas onto a substrate. The powder particles get accelerated and focused through a nozzle to reach super sonic velocity. The moveable nozzle directs the focused particle spray on to a substrate where the particles collide and turn their kinematic energy into plastic deformation and get deposited and joined on to the substrate. In figure 2.6a the basic of cold spray can be seen. An inert gas stream is used to transport metal powder into a pressurized gas chamber where it meets a second, heated inert gas stream which drives the metal powder trough a Laval nozzle and gets accelerated to supersonic velocity and finally hit the substrate respectively the work-piece and get stuck to the surface.

Thus during the process, the feedstock is not melted, different material combinations and integrations can be achieved e.g., aluminium & steel, titanium & copper. Figure 2.6b shows a cooling jacket with integrated cooling channels made by cold spray DED, with afterwards machining, out of two different materials. While the inner copper layer with integrated cooling channels gives good thermal conductivity, the outer layer of stainless steel brings corrosion resistance and strength to the part.

(a)   (b)
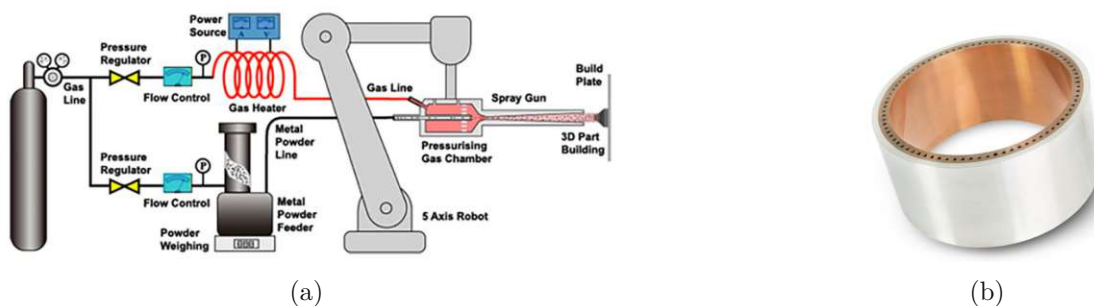
Figure 2.6: (a)Cold spray additive manufacturing set-up by Titomic Ltd., Australia [12]; (b) cold spray DED-demonstrator of a cooling jacket after post processing by Impact Innovations GmbH, Germany [13].

Joule heating

Joule heating, also known as resistance heating is the generation of heat by a conductor which is applied a to potential. For additive manufacturing this phenomenon is used to heat locally applied metal wire which gets molten by the resistance heat. This technology is very similar to gas metal arc welding but instead of forming an electric arc to melt the substrate and the consumed wire electrode the applied voltage gets limited so the formation of an electric arc is suppressed. In figure 2.7(a) the process scheme of joule heating is depicted, (b) shows the proprietary joule printing process by Digital Alloys in action. Joule printing is a relatively new AM-technology, patented by Digital Alloy´s Inc., which benefit lies in the style of energy input into the printed part. Due the wire gets heated directly without the use of an electric arc, or a beam, the generated heat stays on a low level, resulting in a minimum of heat affected distortion of the part. However, an issue joule printing has to deal with is the relatively low quality of mechanical properties due lack of fusion of the printed layers which come from the minimum heat input. What also might be of interest about joule heating is the fact that for the process there is just a minimum of accessories needed and there are no sources of danger like an electric arc or a laser beam, beside the hot metal, thus making it possible to be built as compact desktop printer.

(a)   (b)
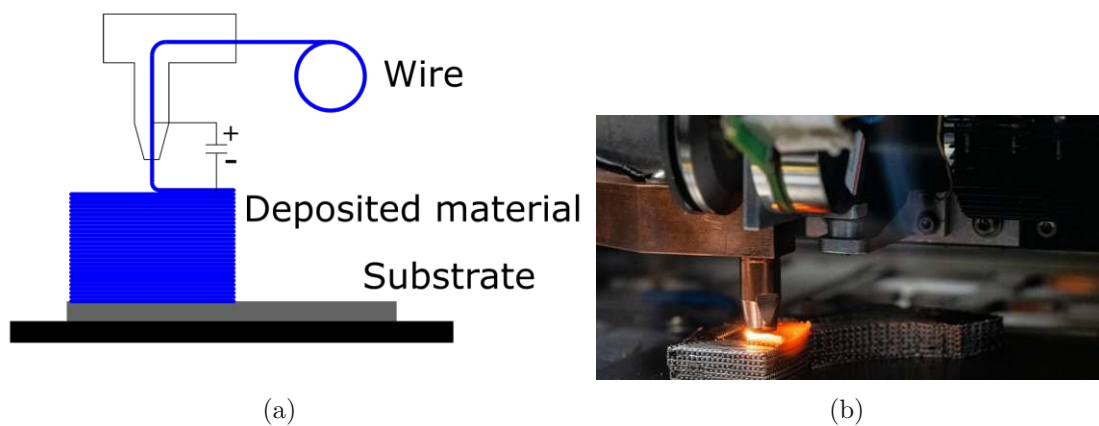
Figure 2.7: (a) Process scheme of DED by Joule heating (b) Digital Alloy´s Inc. proprietary joule printing process in action [14].

Arc based

DED by electric arc is strongly bound to the common fusion welding processes gas metal arc welding, plasma arc welding and gas tungsten arc welding. While GTAW is not that common for DED, GMAW and PAW are. The main differences are that at GMAW the wire (cathode) is consumed during the process and gets transferred into the weld pool, whereas in PAW the tungsten cathode is not consumed but wire is fed from lateral direction into the melt pool. The difference also lies in the feedstock form, while PAW can handle metal powder to be processed, GMAW & GTAW are not common to be used with powder.

Beside arc-based-DED processes have low resolutions, they are not used for high complexity parts but are more suited for sizes starting from 100mm up to a few meters. The main benefit for these processes lies in their reduced material consumption, their well known process and acceptance in industry coming from their welding heritage. Figure 2.9 shows a additive manufactured titanium part made with plasma arc DED. The layer wise build-up and the rough surface can be well seen.
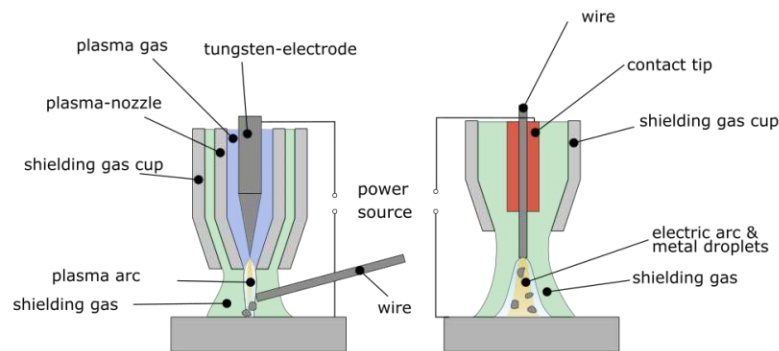
Figure 2.8: Arc based DED processes by plasma arc welding (left) and gas metal arc welding (right) [15].

Figure 2.9: Titanium structure made by plasma arc DED process [15].

Beam based

Beam based DED comprises the both energy sources laser beam and electron beam and similar to arc based DED they have their background in welding respectively cladding and hard facing. Most laser based DED use powder as feedstock form, while the electron beam can solely use wire due the necessity of high vacuum inside the workspace. Figure 2.10 a&b show the principle of both technologies.

Compared to arc-based DED they have higher investment costs, in case of the electron beam it is significantly, but yet do have less wear parts which eventually have to be replaced during processing and also have a more dynamic behaviour of their energy source. Beside the use for additive manufacturing, many laser-DED systems can also be used for repairing, cladding or hardfacing. Figure 2.11 shows a series of pictures from start to the final product of a laser-powder-DED produced fan-frame for an unmanned aerial vehicle (UAV). The printed part shows less complexity which is finally enhanced by a post-processed milling step to get the final part.
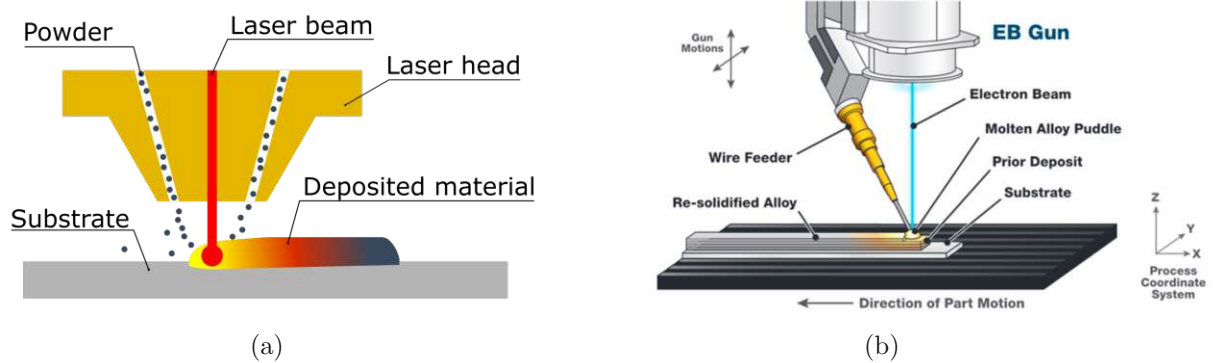
Figure 2.10: (a) Process scheme of laser-powder-DED; (b) Process scheme of EB-wire-DED [16].

Figure 2.11: Productions steps of a fan frame for an UAV made of an aluminium alloy during the FFG project (Austrian Research Promotion Agency) *GenerAl* (FFG Nr. 843981), courtesy of the whole project-consortium [17].

2.3 Users and applications of directed energy deposition

The development of additive manufacturing is strongly driven by international communities, universities, start-ups and institutes. To give an overview of the main players in the DED scene, the following pages will present a selection of stakeholders for R&D, system manufacturers and users.

Leichtmetall Kompetenzzentrum Ranshofen (LKR)

The Leichtmetall Kompetenzzentrum Ranshofen (engl. Centre for excellence of light metals in Ranshofen), a branch of the AIT - Austrian Institute of Technology, is one of Austria´s most pioneering institutes in the field of DED. They offer a broad range of products and services i.e. R&D of material & software, consulting, feasibility studies and prototyping. The material scope are according to its name light metals with focus on aluminium, magnesium and titanium alloys.

Their equipment comprises a GMAW-system, a GTAW-system and a PAW-system in combination with 2 6-axis robots and a tilt-turn table.
The strength of the LKR thereby lies in their holistic approach on R&D of DED. Beside their equipment for doing DED they also have the infrastructure for small batch wire development and production, making it possible to cast a desired metal alloy and press it in wire shape which can be afterwards used for the arc-based DED process. With this strategy LKR is capable to give the research and development of processes and accessories a much broader view than just dealing with one of them and develop optimized process and wire compositions.
In figure 2.12 a feasibility study of 3D printed piston made of an special, self developed 7XXX aluminium alloy (zinc is main alloying material) can be seen [18].

Figure 2.12: Additive manufactured piston made of aluminium, courtesy of LKR GmbH [19].

MX3D

Founded in 2014, MX3D was earning international prestige in October 2018 when they presented their 12m additive manufactured pedestrian bridge on the Dutch design week. Since then they have realized a number of AM-projects for design, heavy industries, marine applications and others.

MX3D is not using AM-systems in terms of off the shelf machines but modified welding robots which are working with GMAW welding technology. They use one or more welding robots simultaneously for printing. Figure 2.13 shows the additive manufactured pedestrian bridge which is dedicated to be used for crossing the Oudezijds Achterburgwal, a canal in Amsterdam´s historic centre.

Their mission is to introduce the advantages of 3D metal printing to industry while their portfolio comprises commercially additive manufacturing services on demand, specific software for programming of robots for DED applications but also complete turn key systems for metal additive manufacturing.

Figure 2.13: Additive manufactured pedestrian bridge for the Amsterdam´s historic centre [20].

Norsk Titanium

Norks Titanium founded in 2004 by Alf Bjørseth and Petter Gjørvad is one of the foremost commercial user of DED technology and a pioneer in DED with plasma arc and metallic wire. They started building their own AM machines to offer AM-contract manufacturing for titanium parts in the aviation branch.

Their proprietary technology, rapid plasma deposition (RPD) works with a special arrangement of two plasma torches and a wire feeding system (figure 2.14a). Two torches, the feedstock and the substrate are connected by two different electric circuits. The pre-heating torch (8) is in circuit with the substrate (1) and preheats the

substrate respectively the before deposited layer by a transferred plasma arc (7). The melter torch (12) is in a circuit via the wire feedstock (3) with the substrate and creates a plasma arc (11) from the torch over the wire to the substrate. The melter (8) melts (6) the fed wire which is further transported due gravity and the plasma arc pressure to the weld pool (5) of the substrate.

In 2017 Norks Titanium was the first company in the world to print certified structural titanium parts (figure 2.14b) for a passenger plane, the Boeing Dreamliner 787[21].

(a) (b)
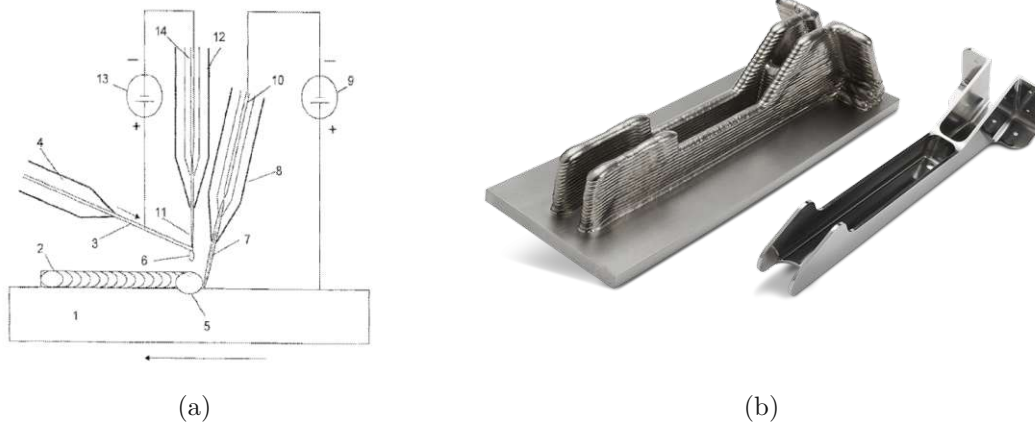
Figure 2.14: (a) Patent drawing of Norsk´s proprietary process RPD [22]; (b) structural part "as built" and finished to be integrated in passenger planes[23].

RAMLAB

RAMLAB (Rotterdam additive manufacturing laboratory) is a consortium owned company by the Port of Rotterdam, InnovationQuarter and RDM Makerspace, based at the port of Rotterdam (Netherlands). Their intention is to bring big space additive manufacturing to shipyards and marine applications by using robots combined with GMAW welding systems. The main driver behind this aim is to significantly reduce port fees of anchoring ships waiting for spare parts by printing the part on site instead waiting some weeks which can cause fees & drops in revenues up to several million Euro [24] [25]. RAMLAB´s first project which got them credits was the printing of a propeller out of a copper aluminium nickel alloy for a tugboat (figure2.15a) of the local port. Another project was the development and 3D printing of a double hook together with Huisman B.V. (figure 2.15b).
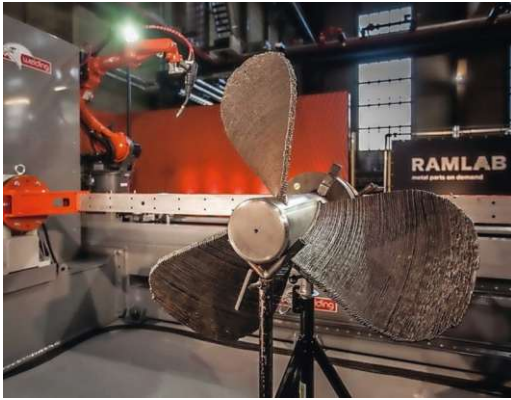
Figure 2.15: Additive manufactured party by RAMLAB: (a) 3D printed propeller for a tugboat [26]; (b) 3D printed hook on the test bench [27].

Relativity Space

Relativity Space, based in California, was formed in 2015 as a spin-off company of Blue Origins, a manufacturer and supplier for rocket technology. Their business concept is to build complete launch vehicles and to manufacture up to 95% of the components on their own by 3D printing. Within this concept they aim for a faster production process, reduce inertia time and the number of components from 100,000 to 1,000 parts per rocket to further make space operations more cost-efficient and accessible to a broader mass. Their 3D printing infrastructure comprises PBF-systems for high complex parts e.g. rocket engines or nozzles and a DED-systems for large and relatively simple parts like tanks & domes. The used DED system (figure 2.16) consists of 3 6-axis robots and a GMAW-system which works in a cell and makes it to one of the largest 3D printer in the world, called Stargate. Their vision is to set up facilities on Mars to print rockets and parts for colonization of space.

Figure 2.16: Relativity Space´s AM-syste Stargate with printed aluminium tank [28].

RHP-Technology

RHP Technology is a 2010 formed spin-off of the AIT (Austrian Institute of Technology) in Seibersdorf (Austria), south of Vienna. The company started with material- & process-development for rapid hot pressing (=RHP) and production of sputter targets for thin films. In 2015 they got into process development of DED by plasma arc and wire respectively powder and formed the proprietary process plasma metal deposition (PMD). Since then they have achieved several research projects with focus on DED. The most significant was a feasibility study to additive manufacture a segment of an optical bench for the ATHENA X-ray telescope [29] which can be seen in figure 2.17. The feasibility study contained development and engineering of the segment with a production of 4 down-scaled demonstrators, two by plasma-powder and two by plasma-wire DED, followed by milling to net shape. Although the sensor bench and the segment never have been made before, neither in additive nor in subtractive way, the potential of material saving was used to show the advantage of additive manufacturing for this application. Table 2.1 shows the difference of the demo part manufactured additively and subtractively. Up-scaling these numbers to the original size of the sensor bench would mean to "produce" 800kg of waste with the PMD process versus 8.6tons of waste with the subtractive process.

(a)   (b)
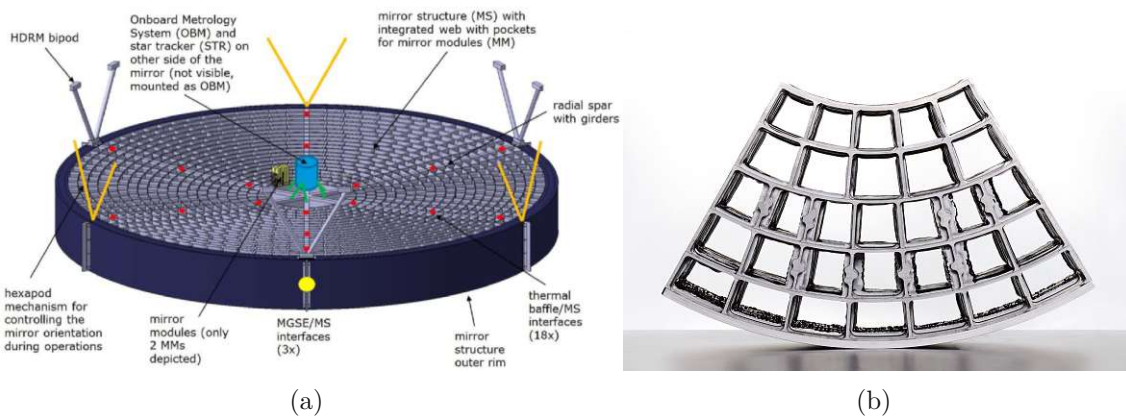
Figure 2.17: (a) Sketch of the optical bench for the ATHENA x-ray mission [30] (b) Additive manufactured segment of the optical bench in cooperation by RHP, AAC & FOTEC.

Table 2.1: PMD vs. machining, casestudy for the ATHENA sensor bench

Demo part	by PMD	by machining
Raw material / final part weight	45kg / 25kg	205kg / 25kg
Waste material	20kg	180kg

SBI

SBI is an Austrian company and a veteran in the field of automation and plasma arc welding and plasma arc cladding. In 2016 the field of additive manufacturing came into the portfolio and was subsequently build up over the next years, resulting in several solutions for plasma arc based DED. The portfolio of SBI comprises DED-turnkey-systems, toolpath planing software for the printing process and process equipment (e.g. welding cameras, plasma torches) for DED. The M3DP (Metal 3D Printer) with a build envelop of 2000*700*800mm and the M3DP-SL (Metal 3D Printer Scientific Line) with a build envelope of 450*450*400mm are the main products for DED-processing of steels, aluminium and titanium alloys. For working with titanium and nickel base alloys the complete working envelope can be flushed with argon to decrease the oxygen concentration down to 20ppm but also to minimize the concentration of moisture and nitrogen within the enclosure.

The offered systems can work with wire or powder material as feedstock but also can be combined by feeding them independently to the plasma DED process.

<div align="center">(a)   (b)</div>

Figure 2.18: SBIs additive manufacturing system M3DP (a) and a printed and partially machined titanium bracket (b) made by the M3DP; [15].

Titomic

Titomic Ltd. is an Australian system manufacturer of cold spray DED-machines. They offer R&D service, metal powder feedstock, and AM contract manufacturing done with their proprietary process Titomic Kinetic Fusion (TKF).

Titomic´s portfolio of DED-machines comprises two products, the TKF9000 with a max. build envelope of 9000mm*3000mm*1500mm and the TKF1000 with a build envelope of 1000mm*1000mm*750mm. While the TKF1000 can print on substrate plates, the TK9000 also can print on revolving substrates such as pipes or shafts which enables additional printing geometries.

Titomic also uses this technology not just to print on substrates like plates, shafts or similar but to print directly on a specific, eventually complex model. This is done by cladding a metal model with a different metal which has an higher melting point then the model. After the cladding is finished the structure gets into an oven where the model gets removed due the lower melting point, leaving the part with the higher melting point.

This process was applied at the bike frame visible in figure 2.19a&b where an aluminium model was coated with titanium and the aluminium afterwards removed. With this technology a seamless bike frame was finally produced.

(a)   (b)

Figure 2.19: (a) Additive manufactured, seamless bike frame out of titanium; (b) bike with the installed bike frame, courtesy of Titomic Ltd. [31].

University of Cranfield - Welding Engineering and Laser Processing Centre / WAAM3D

WAAM3D is a spin-off of the university of Cranfield and is one of the international pioneers of DED. They shaped the - in DED communities - well known proprietary process WAAM (wire arc additive manufacturing), which is sometimes wrongfully used as synonym for wire and arc-based DED. Their starting activities in DED date back in the 1990´s when they developed with Royce Rolls an additive manufacturing process for the production of casting moulds. Their portfolio comprises DED-systems, wire material, feasibility studies, parameter studies, software solutions for DED and consulting. Different to other DED-system providers, WAAM3D offers their systems with either PAW or Cold Metal Transfer (a proprietary GMAW process). Figure 2.20 shows a concept of WAAM3D´s AM-system. A 6-axis robot mounted on the ceiling manipulates the laser head or plasma torch along a tilting table to print the part.

WAAM3D´s R&D focuses on solutions for the - in the UK very strong - aerospace industries like BAE (British Aerospace Electronic Systems), EADS (European Aeronautic Defence and Space) or Airbus and therefore focus on materials like titanium alloys. When it comes to 3D print titanium WAAM3D has a quite different strategy to do so. Due the high affinity of liquid titanium to oxygen, nitrogen and moisture the printing process has to be shielded of the surrounding air atmosphere to prevent unwanted altering of the titanium. This can be done by putting the complete process in an airtight chamber and flush it with inert gas to achieve residual oxygen concentrations of approximately 50ppm or lower. WAAM3D´s strategy to keep the liquid titanium from altering is instead to put just the printing process in a locally shielded atmosphere by putting a large areal shielding device around the plasma or GMAW torch which creates a local inert gas shower.
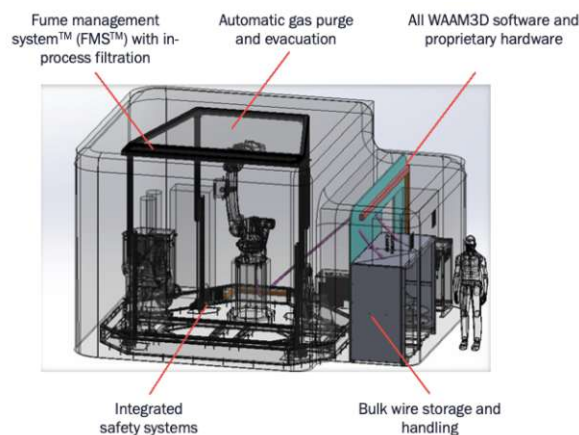
Figure 2.20: Model of a DED-system by WAAM3D [32].

2.4   Plasma arc welding

Plasma (a derivation from ancient Greek which means jelly or mould-able substance) is the fourth fundamental state of matter; according to the Max-Plank Institute 99% of the universe visible matter is in plasma state [33]. It is a gaseous mixture of electrons and highly charged positive ions. To create a plasma one has to heat gas up to several thousand degrees Celsius or to subject gas to a strong electromagnetic field. In the nature we can study plasma during a lightning strike, produced by an electric discharge between the atmosphere and an earth-bound object. Artificially produced plasmas can be used for different tasks e.g., light source (in gas-discharge lamps), medical technologies (for sterilization, plasma medicine for wound curing), chemical applications (plasma-enhanced chemical vapour deposition) and production engineering (plasma cutting, plasma welding). For this work plasma is just relevant for its use as heat source in in arc-based DED applications.

An electric arc is an electric discharge between two electrodes, a cathode and an anode 2.21. Between those two electrodes a current flows through a gaseous medium. The condition therefore is the presence of enough conductive charge carriers and enough potential difference between the electrodes. Under normal room conditions gases are in form of molecules or atoms, to make them conductive they first have to be (if not a noble gas) dissociated and ionized. Table 2.2 shows the dissociation and ionization energies for common welding gases. Note the almost equal ionization energy for argon, oxygen, nitrogen, carbon dioxide and hydrogen and the much higher energy demand for helium. The reason for this behaviour is that helium just owns one electron shell with two electrons which needs more energy to separate an electron from its core. Therefore a higher energy amount is needed which also succeeds in higher arc temperatures.

Table 2.2: Dissociation and ionization energy for common welding gases [34].

Gases	Dissociation eV	Ionization eV
Argon	-	15,8
Helium	-	24,6
Oxygen	5,1	13,6
Nitrogen	9,8	14,5
Carbon dioxide	4,3	14,4
Hydrogen	4,5	13,6

At welding processes the plasma arc is the source of thermal energy, and is therefore
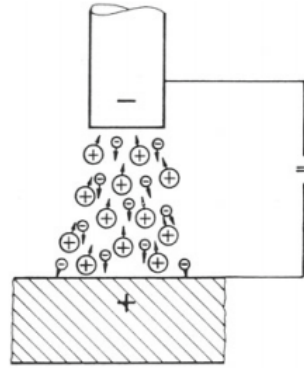
Figure 2.21: Electric discharge of a positively charged substrate (anode) and a negatively charged electrode (cathode); [35, p. 18].

called a thermal plasma. In the electric field between the two electrodes the electrons and the ions are accelerated, electrons to the anode and ions to the cathode. On their way to the anode the electrons are colliding with other gas atoms. The energy of impact is sufficient to ionize these atoms and to release further electrons. This leads to a chain reaction where more electrons are released then recombined. The amount of electrons and ions is a quantity for the grade of ionization and conductivity of the plasma.

Due the difference in mass between electrons and ions, the electrons move much faster in the plasma arc then ions do. When they hit the surface of the anode the kinetic energy is transferred to the molecules of the anode which results in an temperature increase. The energy of the arc is converted into heat energy, the temperature of the arc is governed by the arc current and the mixture of gas between the two electrodes[36]. Depending on the welding technology arc temperatures of 4,000K up to 24,000K can be obtained.

A rough separation of arc temperatures [36] of the corresponding welding processes:

- Plasma arc welding (PAW): 10,000K ... 24,000K

- Gas tungsten arc welding (GTAW): 4,000K ... 10,000K

- Gas metal arc welding (GMAW): 5,000K ... 7,000K

The history of plasma arc welding started in the US in the 1940´s when Russell Meredith of Northrop Aircraft developed a welding process for non ferrous metals foremost aluminium and magnesium, with a non-consumable tungsten electrode covered by a shielding gas cup which releases helium to protect the weld pool of

oxidation [37]. Said process was called Heliarc due the use of helium as inert gas and is nowadays better known under the name gas tungsten arc welding or tungsten inert gas welding (TIG). Based on this technology, Robert M. Gage developed in the 1950´s a new welding process where he put a nozzle with a small orifice diameter over the tungsten electrode and flushed the nozzle and the shielding cup with each separated inert gas fluxes, which increased the energy density of the electric arc and made it possible to weld thicker but also thinner sheets of metal then possible with GTAW [38]. This process is nowadays known as plasma arc welding. The inert gas fluxes are called plasma gas which streams through the nozzle and shielding gas which streams between nozzle and shielding cup. Figure 2.22 shows both, GTAW and plasma arc welding, the similarities of both set-ups are easy recognizable. While the GTAW set-up creates a broad arc and therefore a wide weld pool, PAW creates a small constricted arc resulting in a thin weld pool with high penetration.
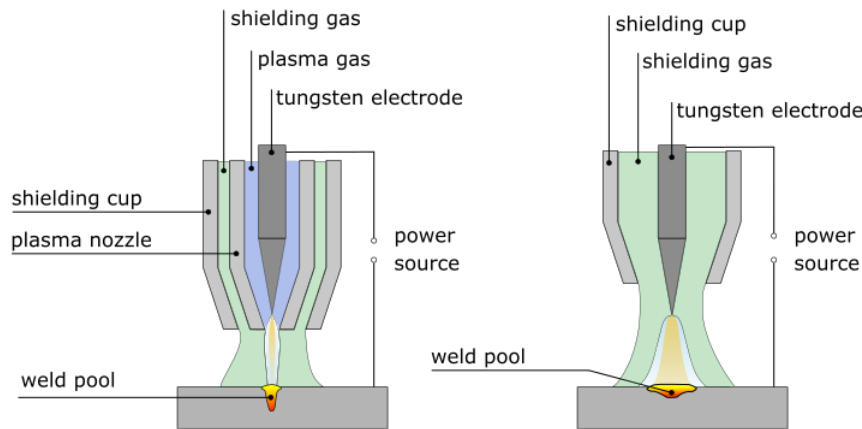
Figure 2.22: Plasma arc welding and gas tungsten arc welding; The constriction of the plasma arc is done by adding a plasma nozzle with a small orifice diameter and by using two separated gas fluxes for plasma (blue portion) and shielding gas(green portion) based on [36, p. 157].

Operation modes of the plasma arc

We already know that one has to create a potential difference between the tungsten electrode and the workpiece to get an electric discharge and further an electric arc. Doing so there are four common circuit forms for plasma arc welding.

- DC straight polarity (DCSP figure 2.23a):
  The electrode is the cathode and the workpiece is the anode; this is the most used mode for DC plasma welding and is widely used for steels (mild and stainless), titanium and nickel-base alloys.

- DC reversed polarity (DCRP figure 2.23b):
  The electrode is pinned as anode and the workpiece as cathode; this mode is used for the occurring cathodic cleaning effect which enables good weld-ability of aluminium and magnesium alloys. A negative effect is that in this operation mode the tungsten electrode has to carry higher temperatures due it is in plus pole and therefore has shorter lifetimes.

- DC combined polarity (DCCP figure 2.23c):
  This mode uses the plasma nozzle as anode and the electrode and the workpiece are used as cathode which enables longer lifetimes of the tungsten electrode while using the cathodic cleaning effect on the workpiece surface which is needed for welding of aluminium and magnesium alloys. Although DCCP gives a better protection of the tungsten electrode its plasma nozzle has to be designed as heavy duty part which might be also the reason why it is rather a niche in PAW.

- Variable polarity plasma arc (VPPA figure 2.23d):
  In VPPA, often called "*AC-welding*", workpiece and electrode are switching between anode and cathode according to a set frequency. While the tungsten electrode is in the plus-phase, the cathodic cleaning effect occurs, while in its minus-phase it has time for cooling. This mode increases the lifetime of the tungsten electrode and is the most common plasma welding mode when processing aluminium or magnesium alloys with the PAW process.

(a) DCSP   (b) DCRP   (c) DCCP   (d) VPPA
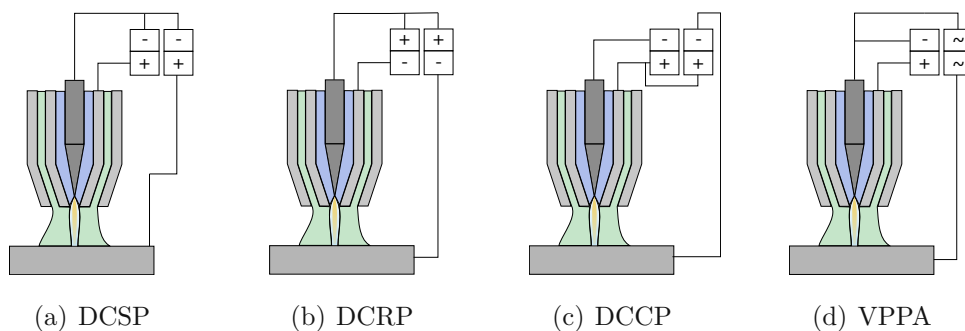
Figure 2.23: The four methods a welding plasma arc can be operated; based on [36, p. 169].

Primarily, the light metals aluminium and magnesium form strong and stable oxide layers with the ambient atmosphere. In case of aluminium, its oxide layer product alumina (Al_2O_3) represents a good electrical isolator and also has a higher melting point then aluminium or its alloys do (alumina: 2,072°C / pure aluminium: 660.2°C). These properties show their negative effects when striking an arc which is harder due the good isolation and the fusion of the workpiece with the filler metal. A method to destroy the oxide layer in-situ is the use of the cathodic cleaning effect.

This effect occurs whenever the electrode is set as anode and the aluminium base material as cathode. While this mechanism was long time not clear how it works, R. Sarrafi and R. Kovacevic describe the mechanism behind this effect [39]. According to their researches a mobile cathode spot which evaporates and destroys the oxide layer is responsible for the cathodic cleaning.

When applying the cathodic cleaning effect in the DCRP mode, most of the heat is created in the electrode due deceleration of the incoming electrons which turns into thermal energy, resulting in low lifetime of the electrode and also in reduced applicable currents. A better protection for the tungsten electrode gives the DCCP mode where the current is transported from the tungsten electrode (cathode) via the plasma nozzle (anode) to the workpiece (cathode). A compromise between using the cathodic cleaning effect and having an arguable lifetime of the electrode is by using the VPPA mode. Due the change between plus and minus pole on the electrode, the cathodic cleaning effect appears during the plus-phase (called hot-phase) whereas in the minus-phase (called cold-phase) the electrode has time to cool down. Typically AC-arcs for plasma welding are operated with frequencies between 50-200Hz. Further the AC current can be modified by shifting the phase-balance. Figure 2.24b shows the phase balance of an AC welding current of 100A with a phase balance of approx. 66% which means during one period the polarity on the tungsten electrode stays 2/3 of the time in minus phase and 1/3 in plus phase. The lower the balance the longer time per period for the positive phase and therefore the better removal of oxides but also the shorter the cooling interval and the life time for the tungsten electrode.

Plasma welding processes

Modern plasma arc welding is a well defined process and divided into several sub-processes according to the EN ISO 4063. The plasma arc itself can be operated as transferred (TA) or non-transferred (NTA) plasma arc. At the TA the arc is
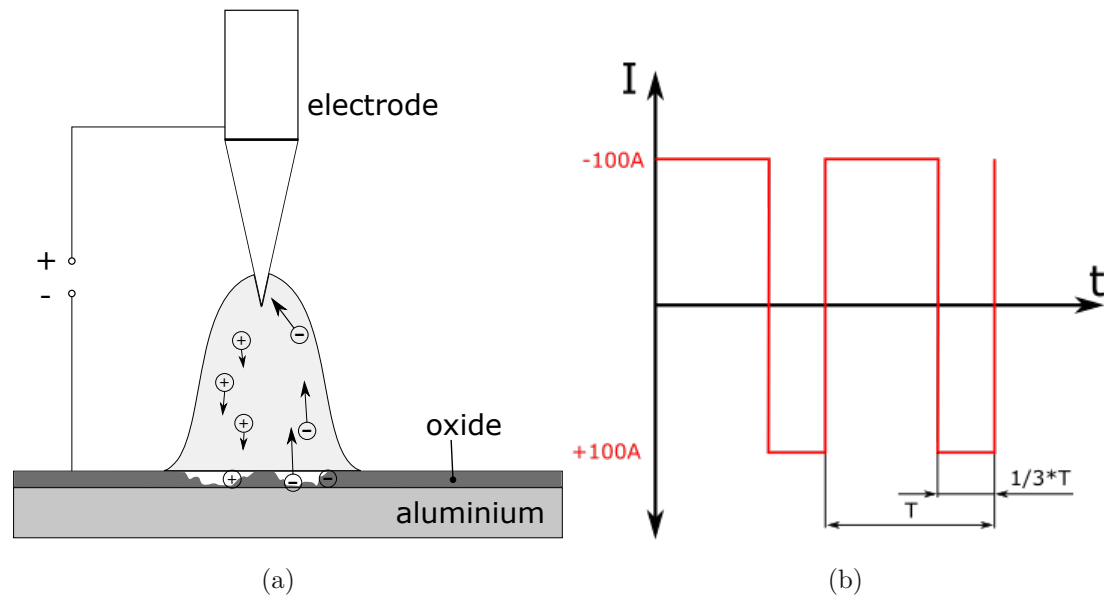
Figure 2.24: (a) Cathodic cleaning effect while the tungsten electrode is the plus pole; based on [36, p. 169]; (b) phase balance during variable plasma arc welding with 2/3 DCSP and 1/3 DCRP during one period.

burning between electrode and workpiece; high temperatures and energy densities are possible. The NTA works with an arc between the electrode and the plasma gas nozzle. The arc temperatures are lower which enables to weld even very thin sheets or non-conductive material. Combining the TA and the NTA brings another advantage beside the benefits of the single processes. The NTA is used as pilot-arc which has an auxiliary function and stabilizes the TA (also called main arc) at low arc currents. Another job of the pilot-arc is to pre-ionize the plasma gas to enable a contact-less ignition of the main arc. According to the standardization EN ISO 4063 plasma welding is titled as process 15; all processes based on process 15 are titled with an additional digit.

- Powder plasma arc welding (process 152 figure 2.25a):
  The powder plasma arc welding process works with a transferred plasma arc. Powder is used for addition and is added through the torch; to transport the powder a carrier gas flux is needed. This process is often used for cladding, and build-up-welding.

- Plasma arc welding (process 153 figure 2.25b):
  This process uses a transferred plasma arc. Due the absence of a pilot arc, the arc ignition has to be done by generation of high frequency voltage or by lift-off ignition.

- Plasma jet welding (process 154 figure 2.25c):

  A non-transferred plasma arc is used for this process, the arc occurs between electrode and plasma gas nozzle. The arc is pushed out by the plasma gas, energy density and temperature are low compared to the other plasma welding processes. This process is mainly used for preheating and welding of non-conductive materials as well as for brazing, soldering and coating.

- Plasma jet plasma arc welding (process 155 figure 2.25d):

  This process combines the above mentioned processes 153 & 154. One arc, the pilot-arc, burns between electrode and plasma gas nozzle, whereas the second arc (the main arc) burns between electrode and workpiece.

(a) process 152　　(b) process 153　　(c) process 154　　(d) process 155
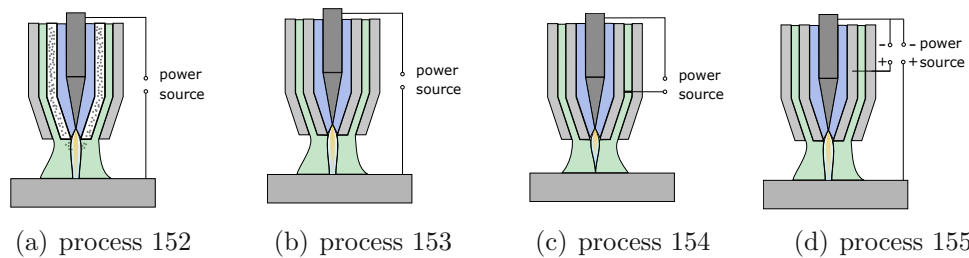
Figure 2.25: Plasma welding processes according to EN ISO 4063 [36, p. 157, pp].

3. Experimental

Within this chapter it will be explained which methods and equipment was used to perform the printing and analysing of the sample walls.

3.1 Experimental gear & wire feed stock

DED-system

The used DED-system for the experimental part was developed, designed and built by SBI GmbH (figure 3.1). The machine is sectioned in a work zone and three electrical cabinets which provide space for electronics, measurement, control and the cooling system. In the work zone a rotational table is placed on a X-Y linear motion system for substrate manipulation while the plasma torch is manipulated by a X-Z linear motions system. Together the axis formed a build envelope of 600mm*600mm*300mm (X*Y*Z). An human machine interface (HMI) allows manual control of the machine in addition a nearby PC gives overview of relevant parameters (e.g., plasma current, plasma voltage, torch cooling temperature) via a software surface.

For creation of the toolpath, the DED-system was programmed by teaching, which is done by defining specific coordinates which are connected to process parameters which are executed when reaching the programmed coordinate. Therefore one layer was programmed and successively offset after each layer in Z-direction. This "master" layer consisted of 6 specific points and can be seen in figure 3.6. During the printing only the X motion system of the substrate manipulation and the Z-axis of the torch was used which finally defined a combined 2-axis motion system in X-Z direction. As power source an AC/DC inverter was used which was capable to deliver a permanent current of 280A. Plasma gas and shielding gas were both electronically controlled by thermal mass flow meters. The wire feeding with a total feeding length of 1m was done by a 2 roll drive (with U-profile) feeder which was positioned approx. 400mm from the plasma torch away.
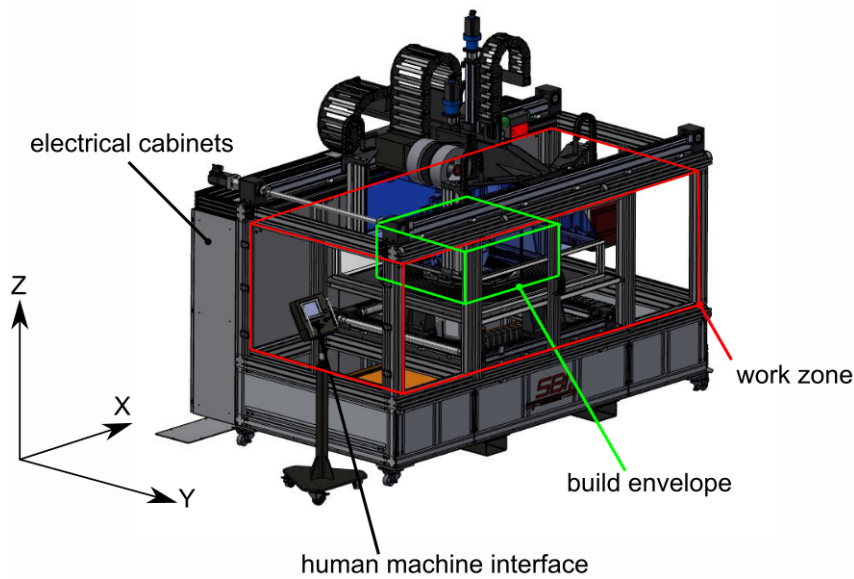
Figure 3.1: Additive manufacturing unit by SBI GmbH

Plasma torch & wire feeding system

The plasma torch is used for creating a plasma arc which is used as thermal power source of the DED system, it is operated as a plasma jet plasma arc welding torch (see 2.25d) switched in VPPA mode (see 2.23d). It was developed and build for a maximum power of 12kVA by a max. welding current of 400A. Figure 3.2 shows the plasma torch together with the wire guide. For the experiment an electrode diameter of 4.5mm and a plasma nozzle with an orifice diameter of 5mm was used. An internal cooling channel directly cools the torch-body while the plasm nozzle was not directly flushed via cooling channels with the coolant.
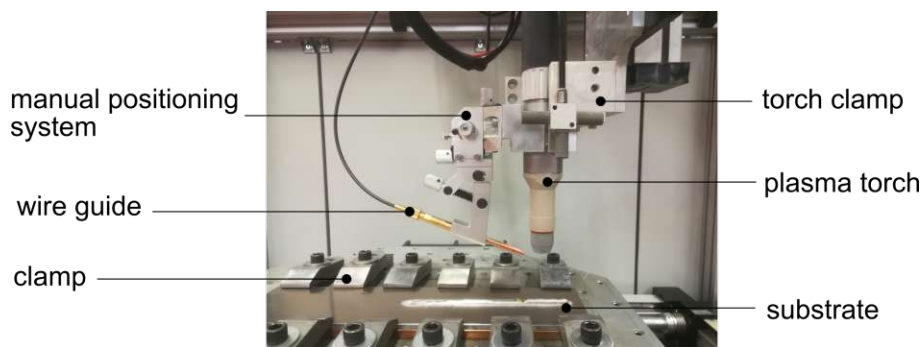
Figure 3.2: Plasma torch and wire guide used for the experiments. The wire gets fed through the grey liner and guided right in front of the plasma torch.

The wire feeder system is the part of the AM machine which is responsible for a constant feed flow. It consists of the wire feeder which drives the wire by coupled rolls and the wire guiding head which directs the wire to the weld pool. The wire

feeder and the wire guide are connected through a plastic liner which leads the wire from the feeder to the guide. Parameters like the wire feed speed (WFS), the bend of the wire liner and the wire diameter can lead to malfunctions. When the WFS is too fast and the bend of the liner is too narrow, the wire grinds on the liner and transfers force to the liner which might results in a wire stuck or can lead to a material abrasion of the liner which gets to the weld pool and affects material properties.

The wire guiding system (figure 3.2) consists of a 4-axes manipulation unit moveable in X-Y-Z and rotatable around an axis parallel to Y. With the axes manipulation a flexible wire positioning can be done. For aluminium the wire was adjusted that it was not hitting the plasma arc directly but rather the weld pool and the previously deposited layer. This feeding behaviour was observed in previous tests to be the best suited which distinguishes in no material spattering and a smooth plasma arc sound.

The gas which is used to create a plasma is essential for the behaviour of the plasma arc. We used argon 5.0 for our experiments which is characterized in its data sheet [40] and consists of 99.999%vol Ar.

Wire feedstock

As feedstock material we used the aluminium alloys EN AW-4043/-4047 & /-5356 for printing the sample walls. The used designation comes from the standard EN 573-1 "*Aluminium and aluminium alloys - Chemical composition and form of wrought products - Part 1: Numerical designation system*" [41].

The numerical designation system for aluminium wrought alloys is structured in the following way:

- EN: **E**uropean **N**orm

- AW: **A**luminium **W**rought alloy

- XXXX: numerical designation of the alloy; the first digit gives the main class which tells the main alloying element, the second digit indicates the modification and the 3rd and 4th digit indicate the specific alloy in the class.

That means the aluminium alloy EN AW-5356 is part of the 5000 class and is the 3rd modification of the alloy 5056. The alloy classes and their main alloying elements are shown in table 3.1.

That said both alloys, EN AW-4043 & 4047 have silicon as their main alloying element and are AlSi5 respectively AlSi12 alloys whereas in EN AW-5356 magnesium

Table 3.1: Classification of aluminium wrought alloys with their main alloying elements.

Series	1XXX	2XXX	3XXX	4XXX	5XXX	6XXX	7XXX	8XXX
main alloying element	99%wt Al	Cu	Mn	Si	Mg	Mg & Si	Zn	others

is the main alloying partner and is an AlMg5Cr alloy. Table 3.2 shows the composition of the feedstock according to its manufacturer [42]. The three alloys were used due their good availability and widely use for welding applications, figure 3.3 shows 1.6mm aluminium welding wire on a basket which was used for the printing.

Table 3.2: Composition of the used aluminium wrought alloys in%wt

EN AW-	Si	Fe	Cu	Mn	Mg	Zn	Ti	Cr
4043	4.5-5.5	<0.6	<0.3	<0.15	<0.2	<0.1	<0.15	-
4047	11.0-13.0	<0.6	<0.3	<0.15	<0.15	<0.2	<0.15	-
5356	<0.25	<0.4	<0.1	0.05-0.2	4.5-5.5	<0.1	0.06-0.2	0.05-0.2
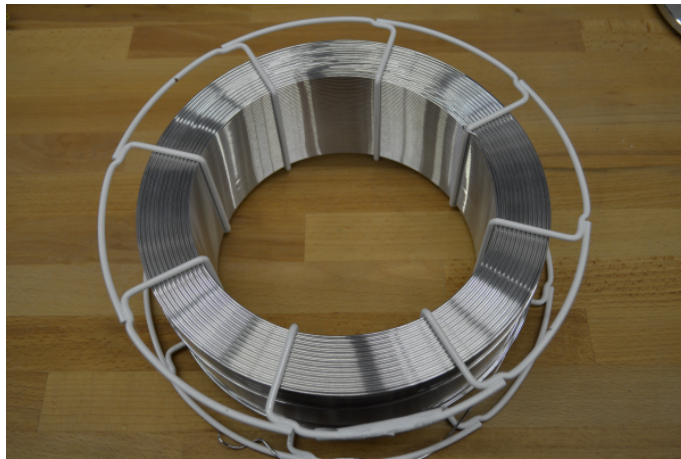
Figure 3.3: Used aluminium wire on a 300mm diameter basket.

3.2 Procedure of experiments

The experimental part was to investigate process parameters on aluminium alloys with focus on their achieved mechanical properties and their quality regarding the occurrence of pores. Therefore 3 aluminium alloys were chosen EN AW-4043, EN AW-4047 & EN AW-5356. While AW-4043 & AW-5356 make about 80% of the total used aluminium filler material [43] they are also often used for wire-based DED due their easy accessibility and good welding behaviour. AW-4047 was chosen due its good printing behaviour in previous tests and the fine looking surface after printing. Based on former experiments and investigations in aluminium alloys we set-up a test procedure pictured in figure 3.4 and which will be explained in detail on the following pages. While the AM processing was done at SBI GmbH, specimen preparation and analytic were done at RHP Technology GmbH.
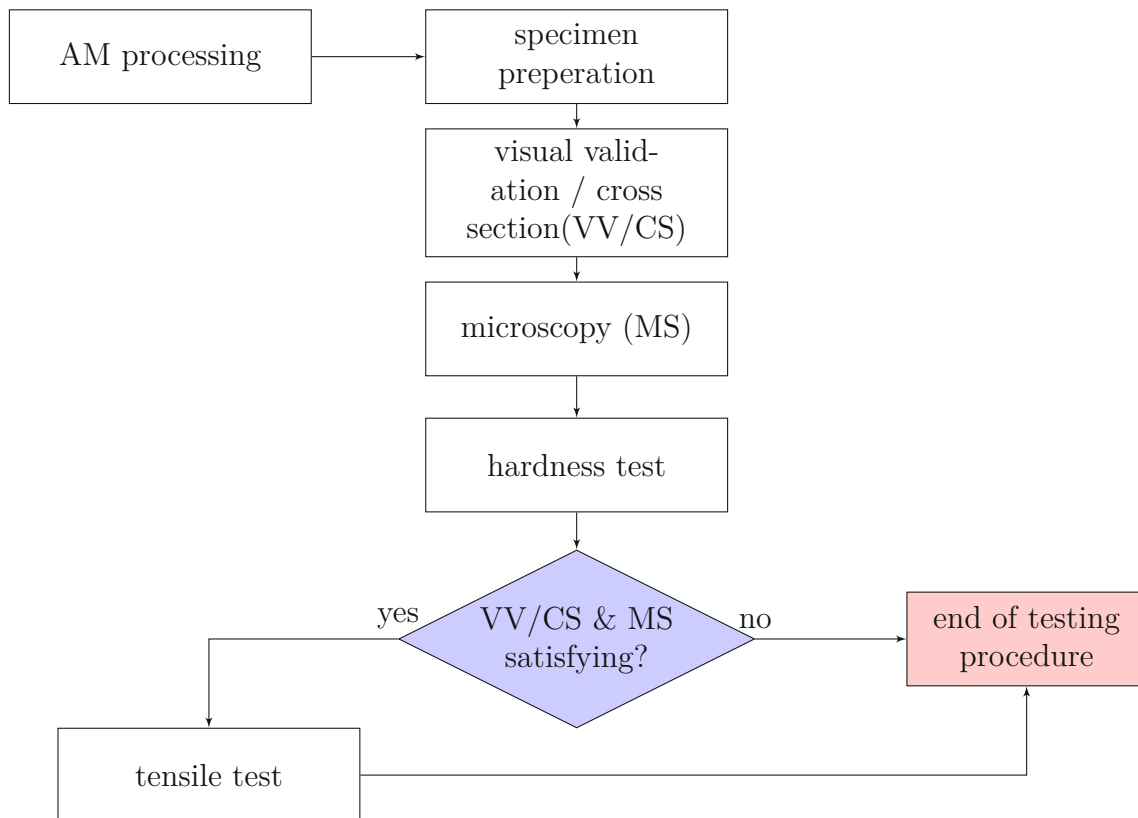
Figure 3.4: Test procedure for examination of the quality of the printed wall structured during this work.

AM processing

At the start a sample wall was designed to give enough space to extract specimen for tensile testing in horizontal and vertical direction as well as specimen for hardness testing and cross section analysis. A sketch of the sample wall can be seen in figure 3.5. Samples walls are commonly used to produce in DED due their easy build up and fast tool path generation.

A total of three aluminium alloys were investigated, EN AW-4043, EN AW-4047 and EN AW-5356. For each aluminium alloy two of those sample walls with different process parameters were printed and afterwards examined thus a total of 6 sample walls was printed (see table 3.3). The difference between the process parameter for each set of alloys was to use a high and a low energy input parameter to see difference in the formation of pores. It is assumed that a higher energy input creates more vaporization of elements and therefore a higher amount of pores in the metal matrix.

Table 3.3: Sample objects & used aluminium alloy with applied energy input.

low energy input		high energy input	
Nr.1	EN AW-4043	Nr.2	EN AW-4043
Nr.3	EN AW-4047	Nr.4	EN AW-4047
Nr.6	EN AW-5356	Nr.5	EN AW-5356
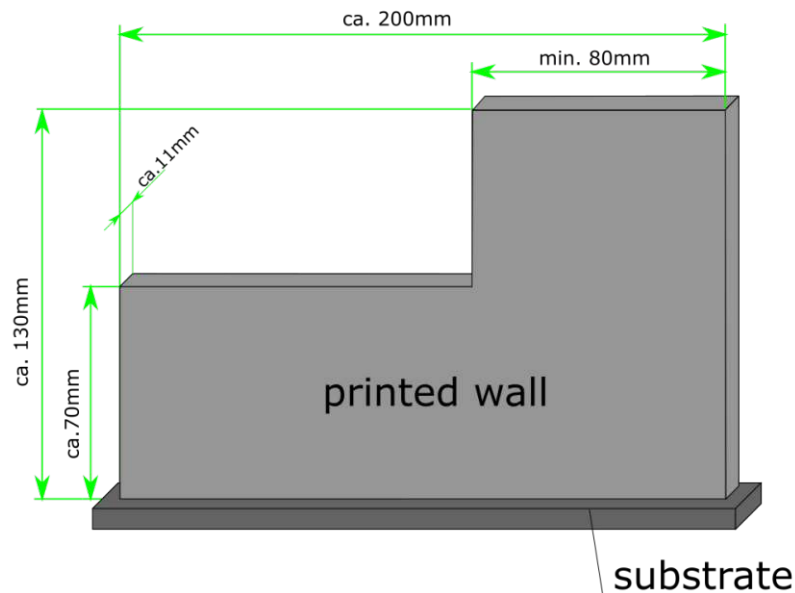
Figure 3.5: Sketch of printed sample wall.

Before we started with the printing of the sample walls, a series of pre-prints was done for finding suitable start parameter and conditions. These were preheating temperature of the substrate plate and the plasma arc current as well as the wire feed speed for the first layer.

Starting with the printing of the sample geometries the first step always was to clean the substrate plates to remove debris, particles and grease which might be on the plates. The plasma torch was equipped with a new set of spare parts which composed of an electrode and a plasma gas nozzle. After the torch was fully equipped it was flushed with argon gas for 5 minutes to get rid of eventually trapped air inside the gas hoses. The flushing time of 5 minutes was determined in a previous test and is the time to reach an oxygen level of at least 50ppm in the plasma nozzle of the plasma torch. In a next step the substrate plate was clamped to the worktable and preheated by applying the main plasma arc to the substrate while moving the same along the substrate. During preheating there was no wire added to the weld pool for depositioning.

When reaching a surface temperature between 200-250°C we started with the deposition of the first layer and proceeded with the following layer deposition until the sample wall was finished. During the whole build-up phase we tried to reduce interruptions due change of consumables, breaks, etc. to a minimum.

The main parameter and info of the printing process are listed in table 3.4.

Table 3.4: Main parameter used for the printing of the sample geometries

Arc current	160-120A	Travel speed	4mm/s
Wire diameter	1.2mm & 1.6mm	Wire feed speed	25mm/s & 50mm/s
Plasma gas flow	1.1L/min	Plasma arc mode	VPPA
Shielding gas flow	12L/min	AC frequency	90Hz
Welding process	EN ISO 4063 process 155	AC balance	75% of period in DCSP

- Arc current
  The current of the plasma arc was used as main parameter and therefore noted

for every sample object and each layer. While starting with higher currents at the beginning of each part, after the first 5 layers the arc current was reduced due to lower heat transfer of the printed aluminium to the substrate plate and the worktable. After the first 10 layers the process reached a steady state and the arc current was kept constant.

- Wire diameter

  For the experiment different wire diameters were chosen due availability. For EN AW-4043 & 4047 diameter of 1.2mm were used whereas a diameter of 1.6mm was used for EN AW-5356. The different wire diameters resulted in different wire feed speed to keep the deposition rate between the printing fo all 6 demonstrators similar.

- Plasma gas flow

  The plasma gas was kept at 1.1L/min which resulted in combination with the 5mm orifice diameter of the plasma nozzle in a soft plasma arc pressure which is essential to keep a stable weld pool.

- Shielding gas flow

  To shield the liquid aluminium from oxidation a constant shielding gas flow of 12L/min was used. To ensure best shielding a 4 seconds pre-flow and post-flow was used before arc ignition respectively after arc shutdown.

- Welding process

  Plasma jet plasma arc welding was used in combination with a variable polarity plasma arc to remove the oxidized aluminium surface in the printing zone.

- Travel speed

  A travel speed of 4mm/s was chosen because at this speed it is still possible to manually react and eventually make countermeasures in case of an error e.g. crash of the torch with the workpiece or weld pool collapse.

- Wire feed speed

  The wire feed speed of 25mm/s (1.6mm diameter) respectively 50mm/s (1.2mm diameter) showed in previous tests good and stable behaviour in combination with the arc current.

- Plasma arc mode, AC frequency & balance

  VPPA with 90Hz was used for the experiments. This value was used due its benefiting influence on the service life of the electrode and the plasma nozzle. By using the 75% AC balance we still had enough plus polarity for a sufficient cathodic cleaning effect while sparing the electrode of overheating.

The applied layer strategy for one layer of the printing process can be seen in figure 3.6 with a description in table 3.5. By superposing multiple layer the sample objects were printed. Point 1 was constructed for positioning the plasma torch on the start point without main arc operation. In point 2 the main arc was activated and a dwell time (DT) of 0.8s was used to create a weld pool without feedstock feed followed by a DT of 0.6s with feedstock feed to start the deposition. Afterwards the torch moved to point 3, the main parameter which are given in table 3.4 were applied between the points 2 & 3 . Points 4 & 5 were constructed to prevent the formation of a hunchback at the end of the wall. After finishing the toolpath for one layer, the height offset was shifted for 1.5mm in positive Z-direction to start the next layer.

Hunch-backing occurs due the weld pool has no support at an ending edge and drops. After several cycles this effect forms a hunchback on the end. From previous tests and trials it is known that a small upward with a following backward motion helps to compensate this effect and creates straight ending edges on open geometries (which is respected in points 4 & 5 in figure 3.6). On closed structures like rings this phenomenon does not occur due there is always support for the end point. Figure 3.7 shows two walls made of aluminium, while the upper one was printed with the strategy depicted in figure 3.6 which resulted in even layers the lower one was just made without the points 4 & 5 of 3.6 resulting in the characteristically formation of an hunchback on its end (right side). The inhomogeneous starting edge on its left comes from too short dwell times at the start position.
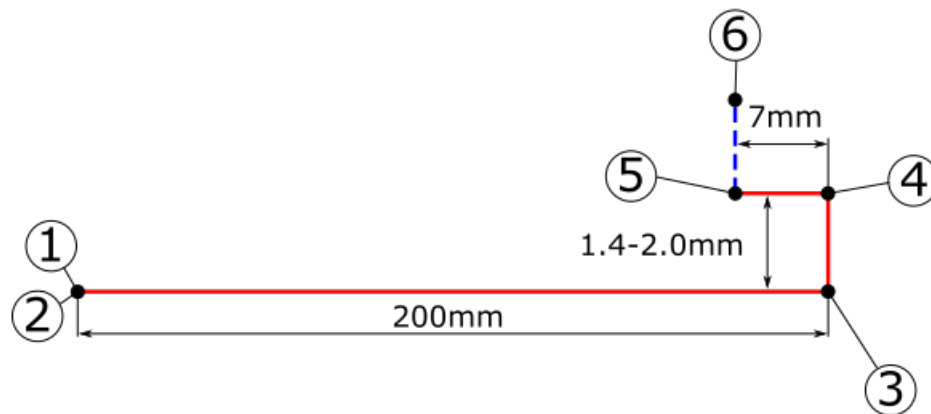
Figure 3.6: The toolpath with its 6 teaching points. The red line symbolizes the path with activated plasma arc and wire feed, while the blue dashed line shows the plasma torch retraction without plasma arc and wire feed.
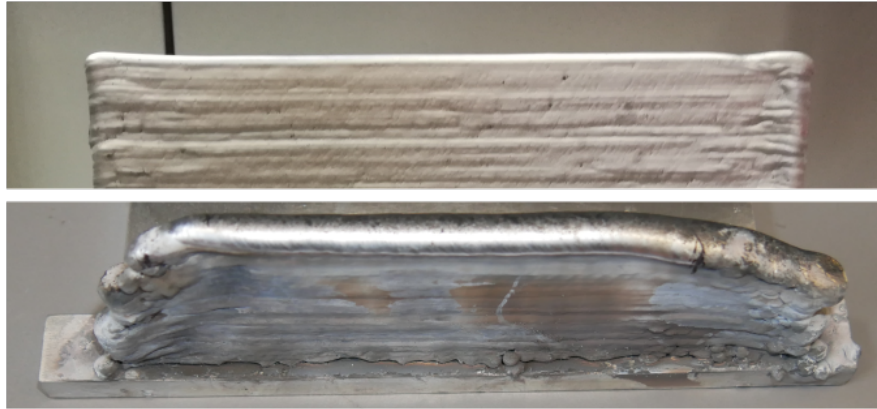
Figure 3.7: Two wall formations made of EN AW5356 (upper) and EN AW6061 (lower) with start point on their left side; upper one made by plasma-DED with hunchback compensation, lower made by plasma-DED without compensation.

Table 3.5: Main parameter used for the printing of the sample geometries. DT=dwell time

Point	Description	Plasma arc	Wire feeder
1	Positioning	off	off
2	Start	on / DT: 0.8s	on / DT: 0.6s
3	Printing of the main portion	on	on
4	Hunchback compensation	on	on
5	Hunchback compensation	on / DT: 0.5s	on / DT: 0.4s
6	Endpoint	0	0

Specimen extraction

After printing of the sample walls they were treated to extract specimen for the following analyse. Therefore the sample walls were cut by wire erosion (electrical discharge machining - EDM). Figure 3.8 shows the schematic sample wall with the specimen to be cut. Specimens 1-12 were used for tensile testing in horizontal (specimens 1-6) and vertical (specimens 7-12) build direction of the wall. To prevent affections of the substrate and the start and end points which are on the left and right edges the specimen were placed with 15mm distance from the substrate respectively 20mm from the left and right edges. For visual examination and also to get an impression of the whole build up a cross section (specimen B) was cut from the walls. Finally a small quadratic plate (specimen A) with 10x10x2mm was cut for hardness testing and crosssection .

In figure 3.9 a detailed scheme for cutting the tensile specimen can be seen. First a bulk portion was wire eroded out of the complete wall. In a second step this bulk portion was clamped and cut in parallel direction and in a third step finally cut loose from the annex. Each bulk portion was processed to get 3 tensile test specimen.
The chosen cutting direction by wire erosion was to keep the testing area of the tensile specimen free of eventually occurring burrs at the edges. After the wire erosion the surface showed a roughness of Ra $3.6\mu m$.

Visual validation and cross section

After printing, the walls and after cutting, the specimen B in figure 3.5 were validated by controlling the macro-porosity, shape, surface smoothness, surface oxidation and discolouration and further as indicators for next analysis. Also part of the visual validation was to compare the dimensional homogeneity of the printed structures by photographing the specimen B and to fit a rectangle with maximum area into the cross-section. By putting the area of the rectangle in relation to the cross-section a parameter, called the area-yield was calculated for describing the geometric quality of the printed wall.

Microscopy

The prepared specimen were examined with a Keyence VHX-5000 to get information about distribution, geometry and size of occurring pores (figure 3.11a). The specimen for microscopy and hardness testing were extracted by wire electrical discharge machining and further embedded in Bakelite respectively epoxy. In a next step the specimen were ground with 80-320-800-1200-2500-4000 papers and finally
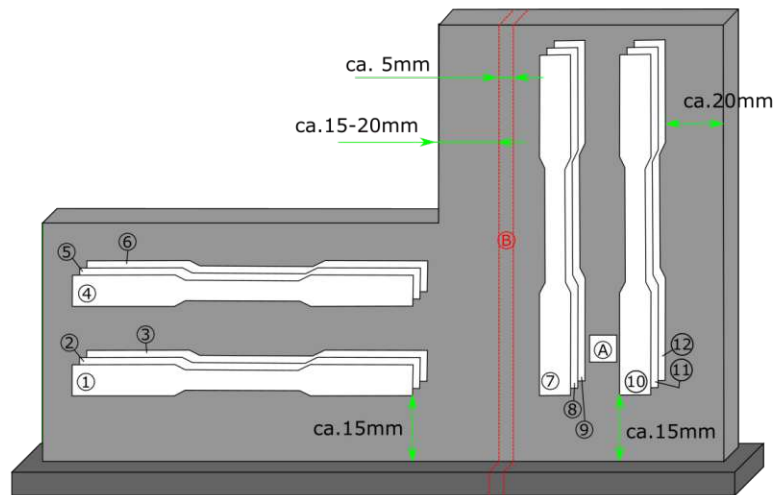
1-12: Tensile test samples
A: Sample for hardness testing & metallography 10x10x2mm
B: Sample for visual cross section analysis

Figure 3.8: Placement of specimen extraction of the sample walls. The step shape was used to extract both, horizontal (Nr.1-6) and vertical (7-12) specimen for tensile testing.

polished with diamond suspension $3\mu m$ - $1\mu m$.

Hardness test

Testing of micro hardness was done with a Qness Q10M (figure 3.11b) with Vickers testing method at 1 kilopond test load and 5s testing period according to EN ISO 6507-1. Specimen A, pictured in figure 3.8, was used to be 10 times tested in line formation while visual detectable pores were avoided to be part of the test area. Figure 3.10 (a) shows the pattern of hardness testing on the specimen.

Tensile test

A total of 12 tensile specimens were extracted and prepared, 6 in horizontal and 6 in vertical direction. The testing was done with a 5kN Testometric testing machine and an Epsilon extensometer with a gauge length of 25mm by a test speed of 20mm/min. The specimens were also extracted by wire electrical discharge machining (EDM) of the sample wall and directly used for the tensile testing. Figure 3.10 (b) shows the used tensile specimen for the test and their dimension. The flat form was chosen due easy extraction by wire EDM directly out of the sample wall.
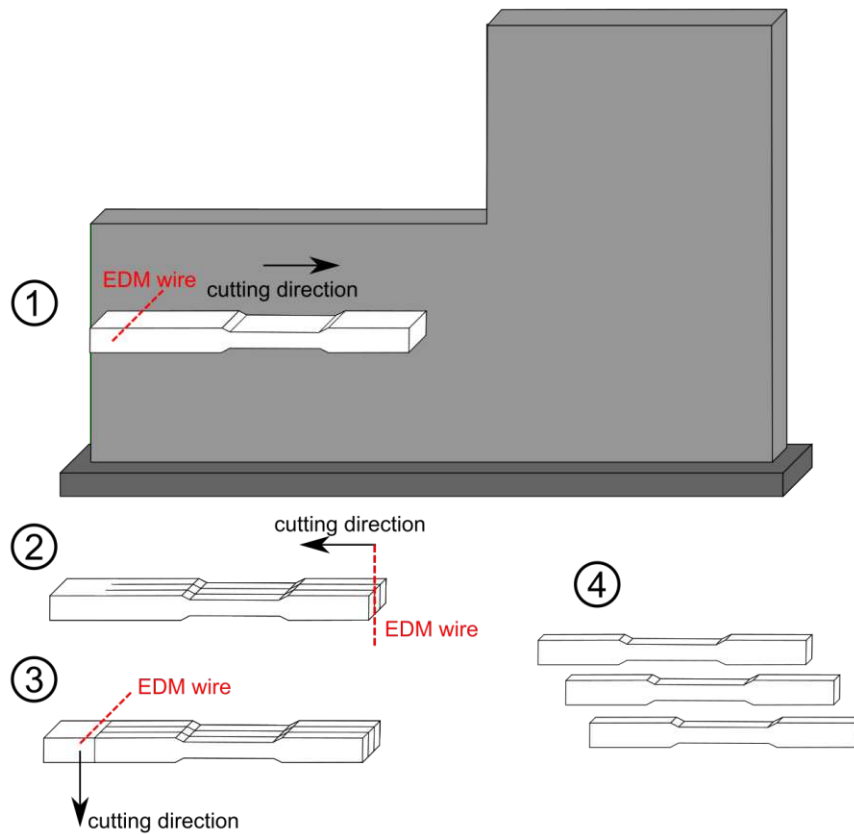
Figure 3.9: Cutting strategy of specimens for tensile testing. At first (1) a bulk portion is cut from the wall which is secondly (2) sliced parallel and later (3) cut from the residual bulk portion which finally (4) gives a set of 3 tensile specimens.
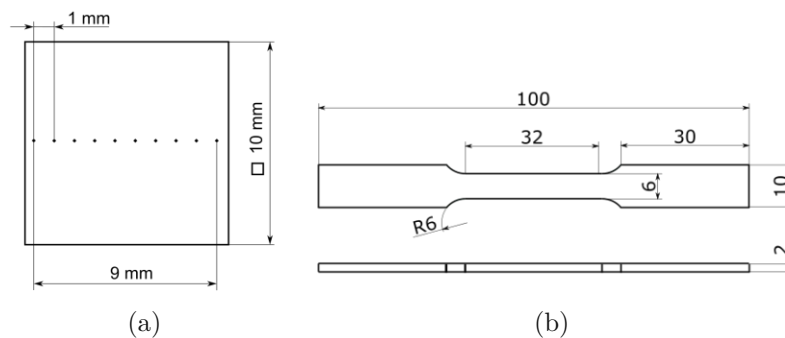
Figure 3.10: (a) Testing pattern for the Vickers hardness testing; (b) Geometry of the tensile specimen.
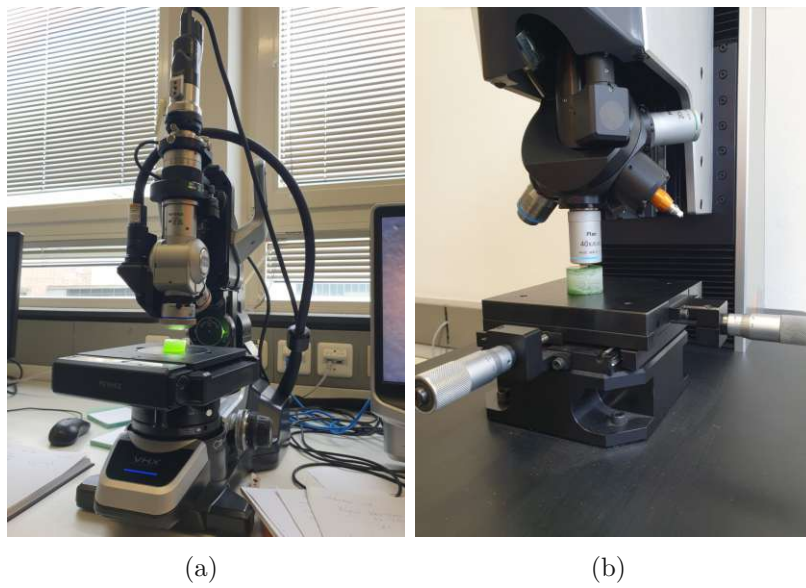
Figure 3.11: (a) Microscopoy by Keyence VHX-5000 and (b) Vickers hardness testing by Qness Q10M with specimen B of object Nr. 6

4. Results

A total of 6 aluminium sample walls were printed, differing in alloy (EN AW-4043 / -4047 / -5356) and used process parameters. During the printing the behaviour of the material and also the plasma arc stability was monitored and noted. Afterwards the sample walls were photographed and specimen for cross section analysis, hardness testing and tensile testing were extracted and prepared by grinding and polishing. On the next pages the results of all 6 walls are presented, starting with the visual validation, proceeding with cross section analysis, hardness testing and tensile testing.

The used process parameters for the sample walls were logged and used for calculating the energy input of the process. Therefore the parameters of the steady process (after approx. 10 layers) were used for calculating the energy input (EI) with following equation:

$$EI = \frac{U*I}{TS} * k$$

U and I are the voltage in V respectively the current in A during the welding, TS is the travel speed in mm/s, k is the factor for relative thermal efficiency and is depending on the used welding process [44] for GTAW and PAW $k = 0.6$. The relative thermal efficiency factor k is defined by how much of the energy input of the arc or the beam is transferred to the workpiece with $k = 1.0$ as reference for submerged arc welding. The low value for GTAW & PAW is based on the fact that for both welding processes, energy is used for the heating of the tungsten electrode and thermal radiation of the plasma arc which is not transferred into the weld.

Table 4.1: Sample objects & used aluminium alloy with applied energy input.

low energy input		$\frac{J}{mm}$	high energy input		$\frac{J}{mm}$
Nr.1	EN AW-4043	504	Nr.2	EN AW-4043	564
Nr.3	EN AW-4047	330	Nr.4	EN AW-4047	402
Nr.6	EN AW-5356	283	Nr.5	EN AW-5356	360

4.1 Printing of the sample walls

Tool path planning

As mentioned before, the tool path planing was done by defining individual points combined by parameters, called teaching. This style of planning is commonly used by robot welding where a robot is doing the torch manipulation and allows a quick creation of the tool path by moving the tool center point of the robot from point to point and teach these coordinates to the controller, therefore called teaching. The benefit of using teaching is that no geometrical info of the workpiece is needed due the tool path planning is made directly on the workpiece. This benefit is in force when doing joint welding. When doing DED there is no workpiece at the start and the teaching of the coordinates has to be done in an approach by estimating the same. While this is feasible for a tool path of one line (for one layer), consisting of 6 points as we have used in this work, it gets more complex if the geometric complexity changes e.g., from a wall (one line per layer) to a block (multiple lines per layer respectively oscillation movement). Further when not only one layer shall be programmed, but all layers for the whole part, the effort gets quickly too high. At some point making tool path planning by teaching is not efficient any more and the use of G-code programming is getting convenient. Another reason why it is of benefit when using G-code at a more complex part is that changes can be done faster and effective then in teaching. However for making a wall it is sufficient for using teaching, programming any other geometrical form of the whole part, G-code is the way to go.

3D printing

The process of printing the sample walls was done by shifting the tool path made by teaching for each layer by 1.2mm in positive Z-direction and start the welding. During the welding changes in the distance between the torch and the build surface sometimes had to be done manually. At the sample walls Nr.2 and Nr.5 the wire got stuck in the weld pool at the layer end which cause a misalignment of the wire feeding angle which had to be readjusted manually either during the welding or between the change from one layer to the next. The used filler wire baskets were sufficient and there was no change of wire within the printing of one separate sample wall. The used tungsten electrode and the plasma gas nozzle was changed whenever a new sample wall was started, within the printing there was no change of these spare parts.

Sound and visual behaviour of an electric arc for printing applications are quick

indications for process stability and defects. This correlation is analogous in the welding branch where seasoned welders recognize from the sound of the arc which defect might have occurred e.g., pores or lack of fusion.

The varied polarity plasma arc in combination with aluminium as feedstock and substrate showed high sensibility to influence from oxygen of the surrounding atmosphere which resulted in loud and inhomogeneous spatter of the arc and further indicated the eventually formation of oxides on the printed surface. Later, after the printing the oxidation could be seen in form of scurfy, discoloured surfaces in the colours of yellow, black and dark grey.

Feeding of the aluminium wire also showed to be vital for the process stability. Fed to the plasma arc it resulted in sputtering of aluminium droplets across the work space and further in discontinuous material deposition on the substrate. Although this behaviour was quickly corrected by manual correction, it appeared sometimes within all of the six sample walls and showed that the chosen parameters and settings are not suitable for a stable, autonomous process. The ideal material deposition of the wire was to feed the same just in front of the weld pool and the plasma arc. By doing so, the wire contacted the substrate respectively the wall just before the weld pool and the plasma arc. Therefore the smelting of the wire was due the combination of heat transition of the substrate (resp. previous deposited material) and the heat radiation of the plasma arc.

4.2 Visual validation and cross section

Table 4.2 shows photos of all 6 sample walls in chronological order. By comparing the geometrical result one can see the rather inaccurate and rough surface of the parts Nr.1 & Nr.2 (table 4.2) to the rest of the sample walls. The sample wall Nr.2 also shows irregular, wavy layers and residual wire feedstock which sticks to the part on the right edge.

During the printing process of Nr.1 & Nr.2 the arc made inhomogeneous spatter sounds which indicated an insufficient shielding of the plasma arc from the air atmosphere. This might come from a too high plasma arc energy which evaporates alloying elements and creates vortexes inside the shielding gas which further brings air into the plasma arc which creates the unstable plasma sound and plasma arc.

The sample walls Nr.1 & Nr.3 showed on their top layers irregularities which can be described as a pin. During the printing process the formation of these pins was

observed in the solidifying area of the just printed layer. Adjacent to the weld pool these pins popped up within a split of a second and solidified. Figure 4.5(a) shows the pin formation during welding while (b) depicts the solidified pin after the printing.

The sample walls made of EN AW-4047, Nr.3 & Nr.4, depicted in table 4.2 show a much smoother surface than Nr.1 & Nr.2. Interestingly the walls do differ in their surface colour, while Nr.3 shows a shiny surface, the one of Nr.4 is matt and pale. When welding aluminium with suitable parameter the bead is shiny and with a smooth surface, while parameter with too high energy input might cause boiling of alloying elements. This leads to an uneven surface with small pins caused by floating gas bubbles which get trapped when the weld pool cools and freezes. Another sign of extensive heat input if magnesium is an alloying element, is a thin layer of black powder which comes from the vaporized magnesium and aluminium which condense in the ambient atmosphere, oxidise and finally form a black powder near the weld bead. Although the colour of the powder is white, it appears black due the small particle size which acts as light trap [45].

Nr.5 & Nr.6 (table 4.2), made of EN AW-5356 showed the least optical differences between each other and in general good visual quality. Both had a smooth surface without pins which might had given suspicion for pore occurrence inside the printed material. Wall Nr.5 shows a difference in the layer where the "*step*" between big and small portion of the wall occurs. From this layer to the end of the sample wall, the part has a darker surface colour than below. Figure 4.3 shows the backside of Nr.5 and the massively covering of the surface with black powder residue which are magnesium- and aluminium-oxides and comes from the magnesium content of EN AW-5356 (5%wt) which gets vaporized and indicates too high plasma arc energy. However, the occurrence of Mg- and Al-oxides alone do not indicate poor mechanical properties but yet slightly decreased strength due the reduced magnesium content which is a tensile strengthener in 5356.

Table 4.2: Printed sample walls Nr.1-6

high energy input	low energy input

EN AW-4043
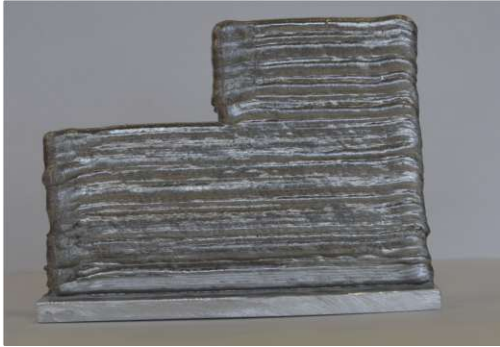
Nr.1   Nr.2
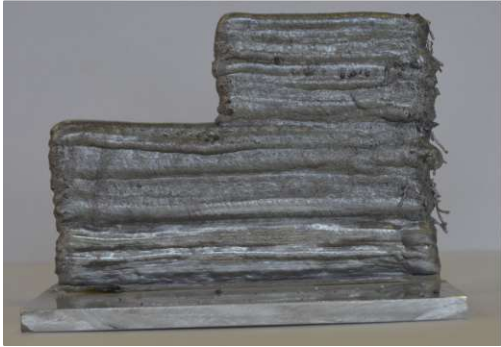
EN AW-4047
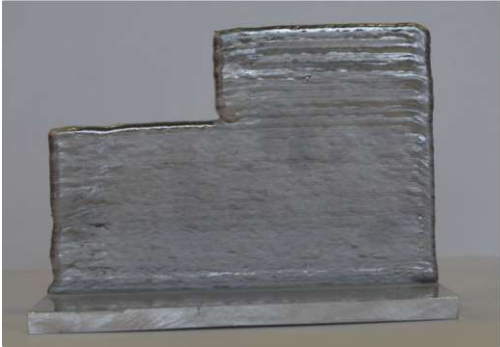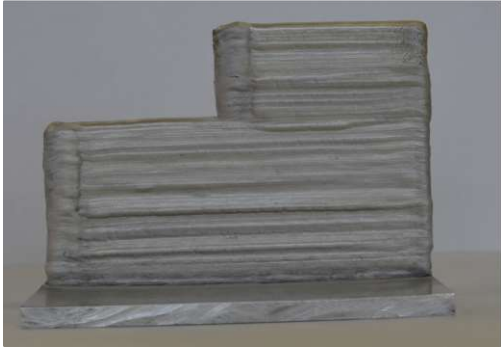
Nr.3   Nr.4

EN AW-5356

Nr.5   Nr.6

An artefact which occurred within all sample walls was the *roofing* of the first layer of the *step* and can be clearly seen at all walls in table 4.2 and detailed in figure 4.2. This behaviour is due the different heat transition situations (see figure 4.1) depending on whether the start point is on an edge (I & II) or somewhere between two edges (III) of the wall. When the start point shift from the edge to the middle of the wall was done, the process parameters were kept constant. Due the increase of surrounding material at the new start point we also had a bigger heat sink which finally led to a narrower weld pool and a smaller material deposition. When the 2nd layer after the start point shift was done the conditions of heat transition turned back to the situation (I) and the weld pool of the start point got back to its previous size and laid above the first start point, creating the *roofing* (figure 4.2).
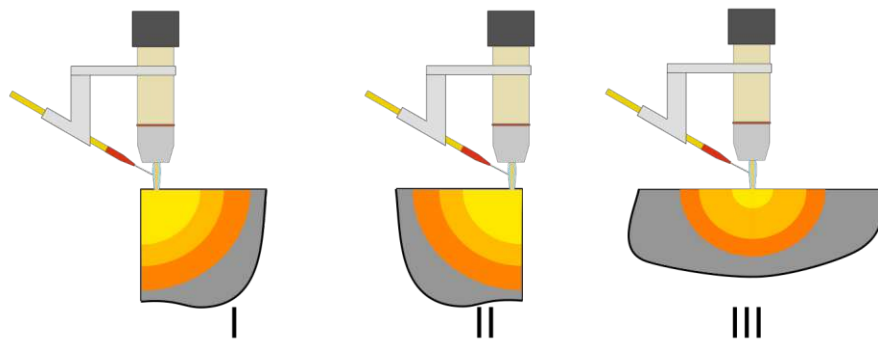
Figure 4.1: Geometrical influence on the heat transition at directed energy deposition.

(a)   (b)
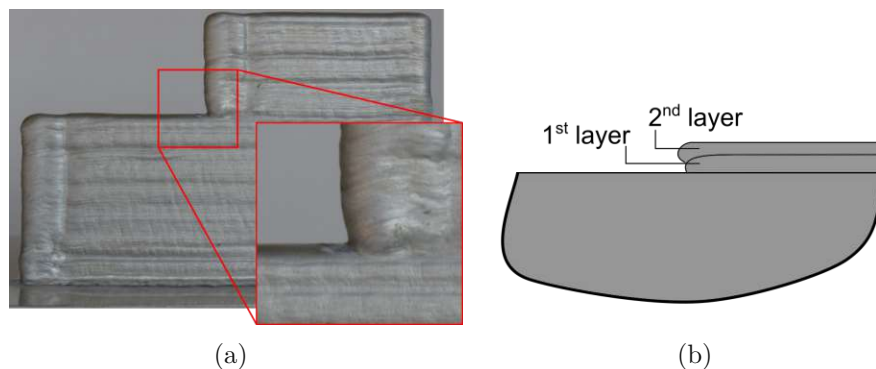
Figure 4.2: Roofing effect in the first layer of the *step*; (a) detail of sample wall Nr.6; (b) schematic build up of the *roofing*

The sample walls Nr.2 and Nr.5 do show the process error of stuck wire material of some layers and can be seen in figure 4.3. While on wall Nr.5 the occurrence is minimal and comes at some start & end points , it is massively on wall Nr.2. This error is caused by two effects (depicted in figure 4.4). If the wire gets stuck by the

(a)   (b)
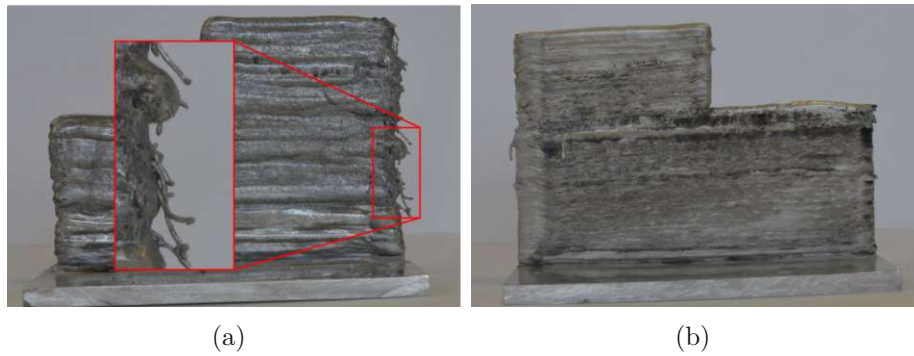
Figure 4.3: (a & b) Wire material which got stuck to the deposited material on sample wall Nr.2 and Nr.5, (b) black soot on the backside of wall Nr.5

start of a layer it is due too fast wire feeding (right side). The wire sticks trough the weld pool and gets smelted from the fed wire, resulting in a stick out from the start point of the layer. In the other case, the wire retraction was too late (left side). Whenever the plasma arc is commanded to stop, there is a delay of 0.4s within the wire feed is stopped and the wire retracted for 5mm. If this time window is not suiting to the layer height which was deposited the wire retraction is too short and can get stuck in the solidified weld pool.
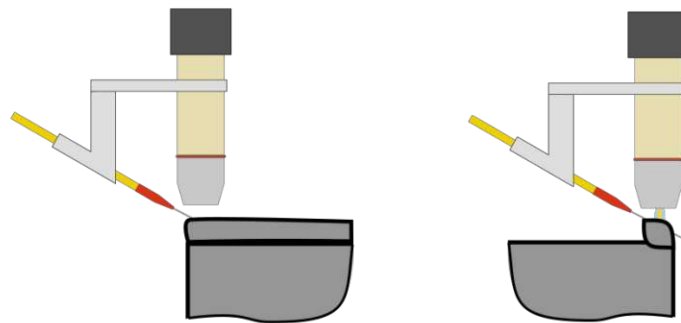
Figure 4.4: Sticking of the wire on the deposited layer. Left (layer end): due low retraction distance of the wire; Right (layer start): due too high feeding speed of the wire.

Beside *roofing*, another effect was be observed on all printed walls, see figure 4.2 - the dog bone effect (due its half shape of a dog bone). This came due the set tool-path described in figure 3.6. The dwell time of 1.4s (=0.8s for the plasma arc and 0.6s for the wire feed) at the beginning of each layer is responsible for this occurrence. Although it is a geometrically flaw, the creation of a dog-bone simplifies the process in its stability and therefore was accepted by the author. Doing a dog bone at the start of each layer supports the process in two ways; first, the dwell time of the plasma arc preheats the starting region and creates the weld pool and second, the

dwell time of the wire feed deposits enough material that no hunchback is created.

A discontinuously appearing geometrical flaw was the necking of layers as can be seen in figure 4.2. The reason therefore was the unsteady inter-pass temperature between the affected layers. In this case the relatively cool temperature did form a small weld pool throughout the layer which resulted in a higher layer hight and a smaller layer thickness, forming the necking which can be seen throughout all sample walls. In the other case a too high inter-pass temperature would support the forming of a lateral overhanging which can be seen at sample wall Nr.2 in table 4.3.

(a) (b)
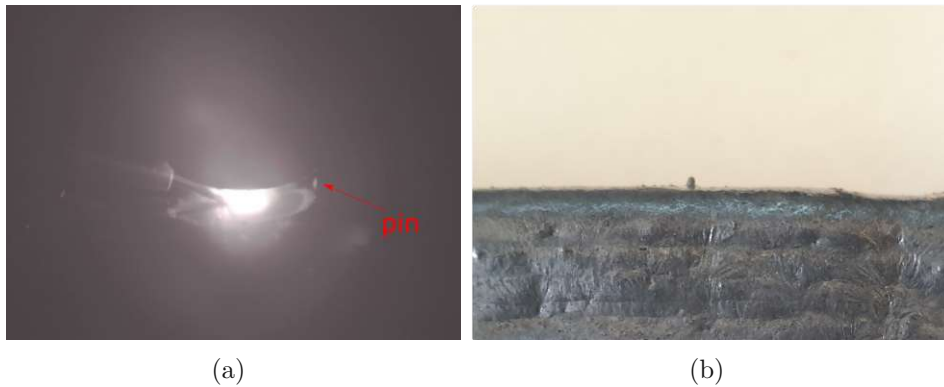
Figure 4.5: (a) pin created by floating gases, (b) pin after finished printing - an indication for pore occurrence in the deposited material

As noted in figure 3.4 the printed walls will be evaluated if their macroscopic integrity is sufficient for a further tensile test. Therefore the cross section (specimen B) of the walls have been analysed for occurring pores or voids which might affect the tensile testing massively. Figure 4.3 shows a comparison of the six wall cross sections in accordance to the used aluminium alloy and the energy input.

The first two walls made of EN AW-4043 Nr.1 & Nr.2 show pores in their cross section. Wall Nr.1 shows a high density of distribution in the lower section next to the substrate plate of big sized pores up to 1mm in diameter which get smaller the higher the wall gets. On the cross section of Nr.2 which was printed with higher energy input compared to wall Nr.1 the occurrence of pores was also visible but yet with smaller sizes. By comparing their geometrical accuracy wall Nr.1 shows an uneven wavy contour and Nr.2 heavy necking and a rather poor link to the substrate plate. Both the mechanical integrity and the geometrical inaccuracy are unfavourable for additive manufacturing application.

Coming to the samples made of EN AW-4047 - Nr.3 & Nr.4 both show similarities

with the previous cross sections of AW-4043. While wall Nr.3, manufactured with low energy input shows lots of big sized pores close to the substrate plate and small sized when moving to the top, wall Nr.4 shows smaller pore sizes which are hardly detectable with free eye. The contour of Nr.3 shows only less wavy sections and has a good link to the substrate. Nr.4 similar to Nr.2 shows an uneven surface with some necking and a poor link to the substrate.

Both sample walls Nr.5 & Nr.6 seen in figure 4.3 show in general good integrity and no pores visible with free eye. When having a look on the contour of all walls, Nr.5 clearly distinguishes by its uneven and wavy contour while wall Nr.6 shows a sufficient steadiness of the same. However, just above the joint of wall Nr.6 to the substrate, necking can be seen which decreases the material efficiency of the sample wall.

Table 4.3: Cross sections of the sample walls Nr. 1-6
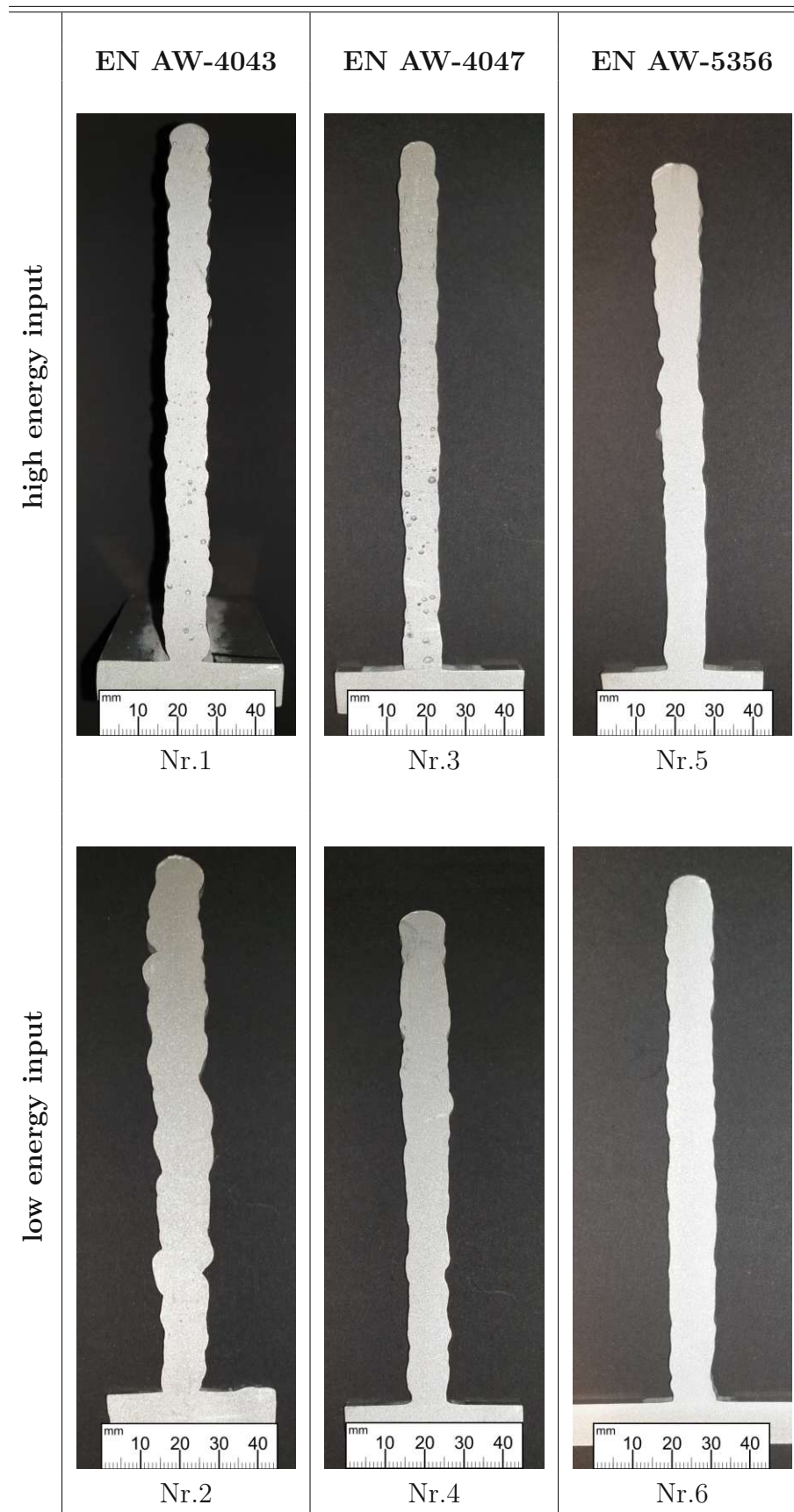
Beside their performance regarding mechanical properties it is essential for DED processes to have a certain degree of dimensional accuracy. A later addition of material in regions with too less material deposited is possible but implicates manual labour, a change of thermal impact and thus a change of thermal stress and also metallography. That said, a later deposition should be the exception and is not representing the idea of additive manufacturing. Additionally by saving time for refinishing, a high dimensional accuracy enables a more efficient printing which is vital for additive manufacturing, especially when printing with high priced materials (e.g., titanium) but also saves time for later machining.

To quantify the geometrical accuracy, the area yield was determined for each sample wall by using the cross-section B (see figure 3.8) which was photographed and further manually redrawn to get the cross-sections silhouette. By adding a rectangular with maximum area into the cross-section the ratio between printed area and rectangular was calculated and used as quality indication for the dimensional accuracy. Table 4.4 shows the analysed cross-sections and their area yield. Although the area yield gives just the dimensional accuracy of the specific cross-section it gives an overall indication of the built part which is evident from the pictures in table 4.2. All sample walls but Nr. 3 do have in common that the first layer has an insufficient wetting of the substrate which result in a limitation of the area yield. Due its massive irregular surface the cross-section of Nr.3 looses lot of area and therefore results in the lowest area yield of all sample walls. On the other hand, the cross-sections with highest area yield, Nr.3 & Nr.6 still show limitations due irregularities in the surface smoothness.

The area yield in general gives advantage to thick-walled structures then thin-walled because the weight of the surface roughness gets lower the thicker the wall becomes. This behaviour is also a reason why DED is more suitable for massive, thick walled parts then for filigree, thin walled parts or features.

Beside the area yield the cross sections of the examined walls show a relevant engineering issue of DED-fabricated parts, the enormous surface roughness which shows max. distances of 2.5mm from valley-hill. This behaviour negatively affects the parts properties for fatigue strength, corrosion and benefits notch effects. Therefore a machining in form of milling or lathing has to be respected in the whole process flow.

Table 4.4: Cross section of the printed walls with inscribed rectangular as quantification of the geometric quality.

Sample nr.	Cross section	Area yield
Nr1		70.1%
Nr2		61.6%
Nr3		73.9%
Nr4		67.2%
Nr5		66.7%
Nr6		75.9%

4.3   Microscopy

The expectations made by the visual validation were partially verified by the microscopy of the specimen. Table 4.5 shows all 6 records of the sample wall´s specimen sorted by alloy and by energy input. Beside Nr.6 all specimen were embedded in Bakelite while Nr.6 was prepared with translucent epoxy which showed to be less suitable for the later microscopy due insufficient contrast. A magnification factor of 20 was used to make the records.

As observed in section 4.2 *Visual validation*, the high energy input wall Nr.1 showed severe pore inclusions - visible with free eye - inside of the printed aluminium alloy. A microscopic view seen in table 4.5, Nr.1 shows a close up of the pore formation. Most of the pores show a spherical shape with diameters ranging from 650 μm (pores 1 & 3) down to $100\mu m$ (pore 4) and one inclusion with vermicular shape and a length of 750 μm. The microscopic record of the sample wall Nr.2 printed with high energy input shows better results. On the observed specimen most pores ranging from 50-120μm while one outlier with 250μm can be seen in (5).

The EN AW-4047 samples Nr.3 and Nr.4 differ as the previous samples Nr.1 and Nr.2. Sample wall Nr.3 shows the biggest pores observed within this work with maximum sizes from 1355μm (7) to 500μm (8) and 180 μm (6). In the specimen of wall Nr.4 the maximum size of pores ranges from 180μm (9) to 100μm (10) and

performed better then its reference specimen with low energy input wall Nr.3.

Finally both samples of EN AW-5356 show porosities which range from $130\mu m$ (11) to 60 μm (12) in wall Nr.5 while a maximum pore size of $150\mu m$ (13) marks the upper limit in wall Nr.6.

Based on the microscopy it can be said that at low energy input we observe bigger pores then at high energy input for both alloys of the 4xxx series. This is also in consistency with studies about aluminium casting where the cooling time is a major effect for the pore size inside the cast aluminium [46]. The higher the energy input the bigger the weld pool and the longer the cooling time to solidify and also the longer the time to give entrapped gases time to leave the liquid smelt.

Table 4.5: Microscopy of specimen A of the printed sample walls Nr.1-6

low energy input　　　　**high energy input**

EN AW-4043

Nr.1　　　　Nr.2

EN AW-4047

Nr.3　　　　Nr.4

EN AW-5356

Nr.6　　　　Nr.5
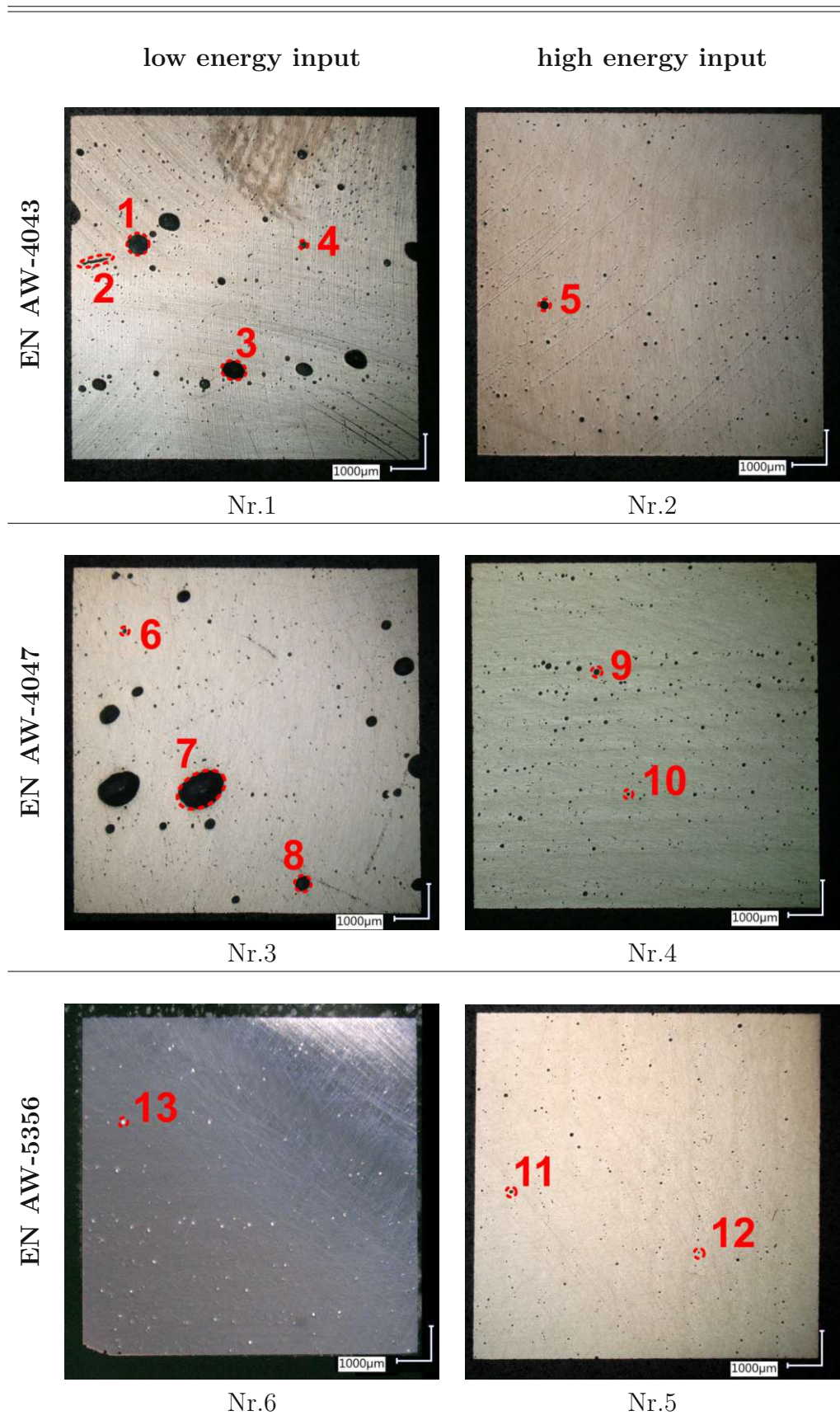
4.4 Hardness test

For hardness testing the same specimens as for the microscopy were used. The test pattern was chosen according to figure 3.10 (a), sos each indentation was separated approximately 1mm. If the intender would hit a visible pore, the proof position was shifted in perpendicular direction. However, most concerning was that hidden pores under the surface would affect the results in hardness testing.

The testing was started with HV 0.1 on a piece of aluminium for reference use. These tests showed that the chosen test load of 0.1 kilo pond was insufficient to create clear edges of the indentation for a robust measuring. Therefore a further reference run was done with a test load of 1.0 kilo pond which showed to be suitable and made clear edges. Figure 4.6 shows stamps of both test loads, note that HV 0.1 (a) was recorded with a focus of 20 and HV 1 (b) with a focus of 40.

In table 4.6 the results of all six tested specimen are depicted and separated in *high energy input* and *low energy input*. The measured values are represented by the blue dots while the red bar shows the arithmetic mean value. Specimen Nr.6-A additionally has a blue-dashed bar which represents the arithmetic mean value exclusively it´s outlier. By comparing the results within the printed alloys one can see that EN AW-4043 high & low energy show differences in their mean value, while both EN AW-5356 specimens show similar values. The massive difference within the alloy EN AW-4047 by Nr.3-A and Nr.4-A just can be explained by an error during the printing of the walls. The similarity of the hardness values of Nr.4-A with Nr.5-A and Nr.6-A imply the possibility that EN AW-5356 was used for Nr.4-A instead of 4047. This assumption will be investigated in the later tensile tests.

(a)   (b)
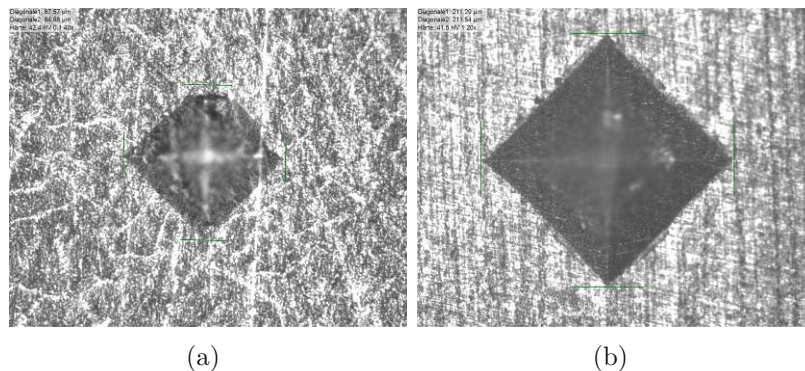
Figure 4.6: (a) Reference testing with 0.1 kilo pond test load (20x focus) and (b) with 1 kilo pond test load (40x focus).

Table 4.6: Results of the hardness testing with a testing load of 1 kilopond at 5 seconds application time on the embedded specimen A (figure 3.8) with dimensions of 10*10*2mm

low energy input	high energy input

Specimen Nr.1-A (EN AW-4043)

Specimen Nr.2-A (EN AW-4043)

Specimen Nr.3-A (EN AW-4047)

Specimen Nr.4-A (EN AW-4047)

Specimen Nr.6-A (EN AW-5356)

Specimen Nr.5-A (EN AW-5356)
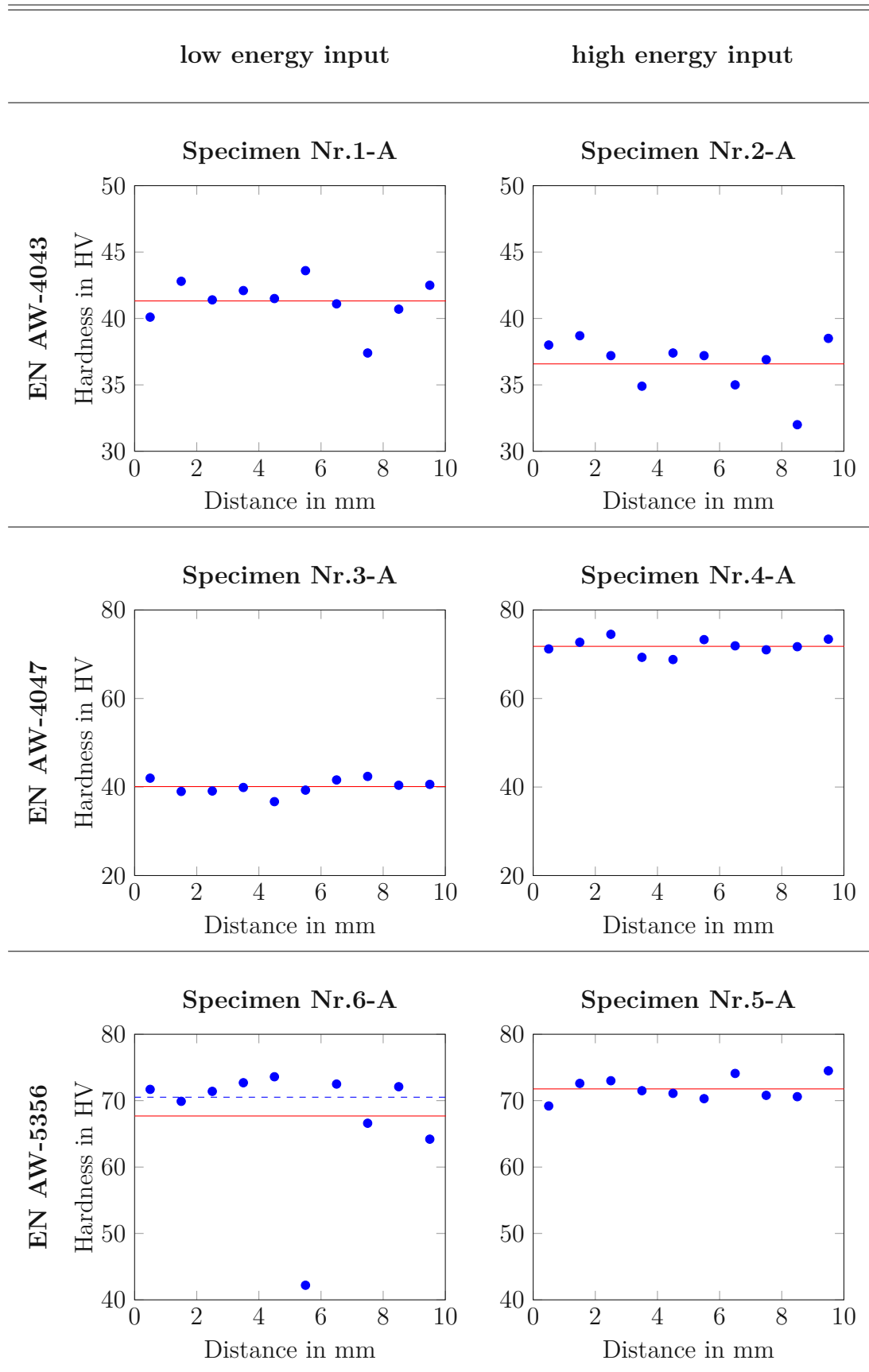
4.5 Tensile test

Based on the results of the visual validation the sample walls Nr.4 / 5 / 6 were used for tensile testing. Due the massive pore formation in the sample walls Nr.1 & 3 these walls were disqualified. Also the sample wall Nr.2 was not used for tensile testing due the unfavourable cross section geometry visible in table 4.5.

The tensile specimen were extracted to examine their performance in vertical and horizontal building direction. In the tables 4.8 / 4.9 / 4.10 the measured, respectively calculated mechanical properties resulting from the tensile testing can be seen. They are separated in a left portion for the results in horizontal direction and in a right portion for the results in vertical direction.

Generally the specimen in horizontal direction showed better mechanical properties than those in vertical direction. This behaviour comes from differing anisotropic character of the printed sample walls.

In table 4.7 the arithmetic mean value of the tensile testing can be seen while table 4.11 shows the measured graphs of specimen in vertical and horizontal direction.

Table 4.7: Arithmetic mean value of Young´s modulus, yield strength, ultimate tensile strength and elongation of sample walls Nr.4 / 5 / 6 in horizontal and vertical direction.

	Horizontal				Vertical			
	E MPa	YS MPa	UTS MPa	A %	E MPa	YS MPa	UTS MPa	A %
Nr.4	$56.1*10^3$	162.1	306.0	20.6	$65.7*10^3$	151.3	287.1	12.8
Nr.4*	$65.8*10^3$	185.0	330.3	20.7	-	-	-	-
Nr.5	$69.9*10^3$	156.9	302.3	20.0	$54.3*10^3$	155.5	283.9	14.1
Nr.5*	-	-	-	-	$63.8*10^3$	156.7	284.8	12.6
Nr.6	$62.1*10^3$	154.3	299.3	19.6	$65.1*10^3$	150.9	272.0	10.2

Table 4.8: Youngs modulus, yield strength, ultimate tensile strength and elongation of Nr.4 EN AW-4047.

	Horizontal					Vertical			
	E MPa	YS MPa	UTS MPa	A %		E MPa	YS MPa	UTS MPa	A %
1	$38.3*10^3$	117.7	259.0	20.2	7	$70.4*10^3$	151.1	281.9	10.9
2	$67.5*10^3$	181.2	331.0	22.3	8	$56.6*10^3$	151.0	275.7	11.6
3	$63.2*10^3$	183.5	330.2	20.6	9	$63.0*10^3$	151.6	280.7	11.7
4	$67.8*10^3$	186.5	330.0	19.4	10	$66.8*10^3$	153.1	290.0	13.2
5	$64.8*10^3$	188.5	330.0	20.5	11	$69.0*10^3$	153.2	295.7	14.5
6	$35.1*10^3$	113.3	256.0	20.7	12	$68.6*10^3$	156.4	298.4	14.5

Table 4.9: Youngs modulus, yield strength, ultimate tensile strength and elongation of Nr.5 EN AW-5356.

	Horizontal					Vertical			
	E MPa	YS MPa	UTS MPa	A %		E MPa	YS MPa	UTS MPa	A %
1	$60.2*10^3$	157.1	300.2	18.6	7	$7.20*10^3$	151.6	279.7	21.6
2	$105.7*10^3$	156.3	302.7	21.4	8	$70.9*10^3$	153.4	273.8	10.6
3	$64.2*10^3$	158.3	301.0	19.8	9	$64.7*10^3$	156.5	285.8	12.5
4	$58.5*10^3$	160.8	307.0	19.6	10	$63.6*10^3$	159.1	292.7	14.2
5	$62.6*10^3$	157.3	303.3	18.2	11	$61.8*10^3$	157.7	287.9	13.0
6	$68.2*10^3$	154.1	299.7	22.2	12	$57.7*10^3$	156.8	283.8	12.6

Table 4.10: Youngs modulus, yield strength, ultimate tensile strength and elongation of Nr.6 EN AW-5356.

	Horizontal					Vertical			
	E MPa	YS MPa	UTS MPa	A %		E MPa	YS MPa	UTS MPa	A %
1	$64.3*10^3$	156.6	298.3	18.7	7	$67.2*10^3$	150.1	261.3	8.7
2	$58.5*10^3$	153.5	295.2	19.3	8	$68.3*10^3$	155.5	281.6	10.4
3	$65.4*10^3$	156.2	302.3	20.8	9	$58.8*10^3$	151.6	266.3	9.6
4	$63.9*10^3$	156.7	302.8	21.2	10	$68.8*10^3$	151.5	279.0	11.0
5	$56.4*10^3$	153.4	294.7	18.2	11	$57.8*10^3$	149.7	278.8	11.6
6	$64.2*10^3$	156.1	302.8	19.2	12	$69.6*10^3$	148.6	264.9	9.9

Table 4.11: Stress-strain diagram of the tested specimens.
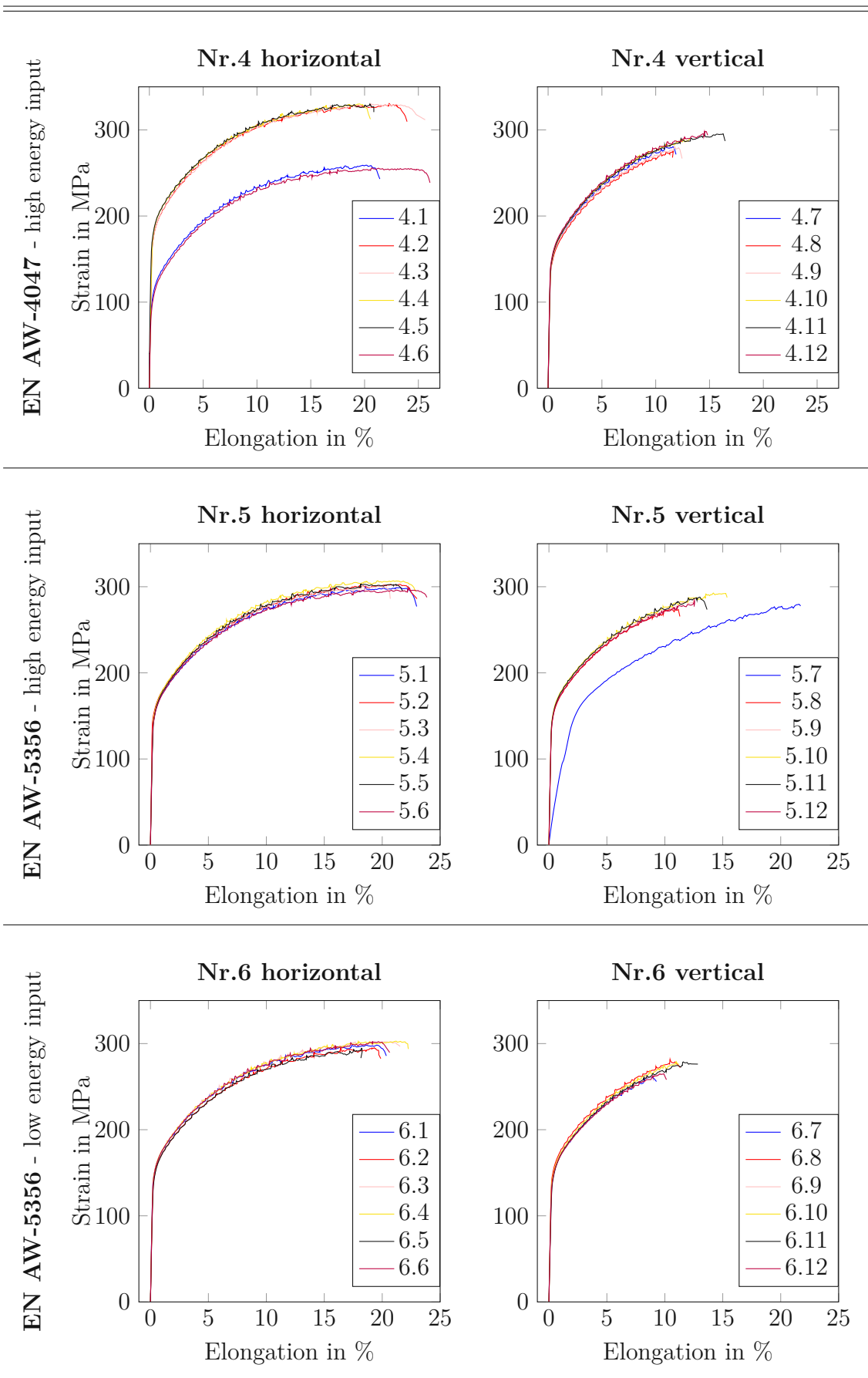
5. Discussion

For this work 6 sample walls of 3 different aluminium alloys were printed with differing process parameters and were further analysed for their mechanical properties but also geometrical accuracy and their suitability for additive manufacturing. Based on the previous chapter 4 Results it can be seen that the achieved mechanical and geometrical properties of the printed sample walls show potential for improvement but also for a critical view which will be discussed on the following pages. Finally the results of mechanical and geometrical properties will be compared to other DED technologies.

AM processing

The whole printing fo the sample walls was done under personal surveillance. This was necessary to manually adopt the printing process which was caused by irregularities e.g., unstable layer height and wire sticking. Due the deposited layer height was not constant, it was vital to manually correct the distance between plasma torch and the build surface. This manually offset correction was done during the process for not creating interruptions in incremental steps of 0.2mm. Most corrections were necessary while printing the walls Nr.1, Nr.2 and Nr.3. The location of the corrections was mainly done at the start and at the end of each layer, while between the points 2 & 3 of the tool path (figure 3.6) there was low necessity for correction.

Not a technically but a safety issue was the formation of ozone during the printing which is especially intensive when welding aluminium. Due the occurrence of UV in the plasma arc spectrum the oxygen of the surrounding air gets reacted to ozone[47], because of low smoke formation during welding the UV rays do not get blocked by the smoke and can also form ozone within a bigger area. Although it was worked with a fume extraction system, it was subjectively recognizable that ozone was present.

Programming of the tool path for one layer by teaching and subsequent superposing after each layer was sufficient, if the whole wall would have been programmed the teaching approach would not be efficient any more and a G-code programming

would have been appropriate. The sticking of the wire within the weld on the walls Nr.2 and Nr.5 did negatively affect the process stability to be automatised, a more robust wire guide would be needed to be not misaligned when the wire is sticking but also a refined wire retraction (e.g., faster retraction and or more wire retraction length) would help to minimize these events.

Geometrical accuracy

Although DED is a rough AM process and dedicated to be afterwards machined to its final shape, geometrical accuracy of the deposited material is an important factor for this manufacturing technology. We used the geometry of a wall in this work thus of its easy geometry which can be programmed and adopted in a short amount of time. During and after the printing of the sample walls we observed a non uniform behaviour of the process manifesting in geometrical differences and as we have seen later also in differing mechanical properties of the printed walls.

For additive manufacturing of more complex parts where 5-axis motions are necessary the used parameter settings of this work will not be applicable foremost due their bad performance of accuracy. Only the parameter setting of sample wall Nr.6 (EN AW-5356) could be used as initial to develop a stable parameter set.

The negative behaviour within the first layer of necking could be solved by changing the parameters within the layer to a higher heat input and therefore a wider weld pool but also by doing a preheating to higher temperatures. Another approach would be to make - analogous to material extrusion (i.e., fused filament fabrication) a brim as first layer. Such a brim could be done by making an oscillation movement instead of a single pass linear movement for the first layer and would preheat the substrate while making a good wetting. Figure 5.1 shows the idea of a brim as first layer.

The generally bad surface quality of the aluminium silicon alloys EN AW-4043 and 4047 assumes the chosen parameter were not suited. A reason might be that the main alloying partner silicon gives the smelted alloy a higher fluidity. Thus, the layer height should be kept low and thus decreasing the deformation of the weld pool by gravity, achieving smoother surfaces.

As mentioned in section 4.2, the printed structures show a high surface roughness after printing. This might be sufficient for heavy industry applications where at some machines, components surface properties play a minor role, but at least a machining of functional surfaces e.g., bolt holes, abutting surfaces or connection interfaces must be done so a DED-fabricated parts can be installed. For light weight engineering or

dynamically stressed applications on the other side, DED-parts have to be subject of a total machining to fulfil engineering requirements for minimal weight, fatigue or corrosion resistance. Beside one of AM and in specific DED most proposed materials are titanium and its alloys which are by a commercially point of view characterized by their high price, compared to steels. Therefore a high geometrical accuracy of the printed part should be reached to minimize chipping material but also the time for machining.
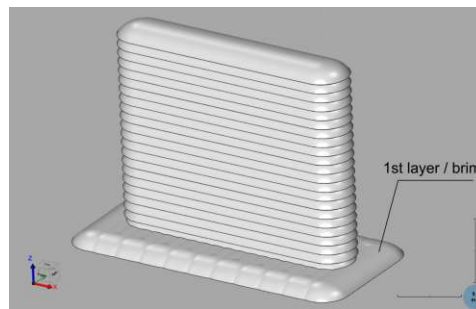
Figure 5.1: Including a brim within the first layer to increase the wetting. In this picture the brim is done by an oscillation movement.

Comparison of the hardness tests done in this work

The hardness testing showed stable values of the tested specimen although the mean values of both EN AW-4043 samples were deviating from apart. When we have a look on the results of the EN AW-4047 specimen we can see a massive difference between both tests. While Nr.3-A is showing a mean value of 40.1 HV 1, Nr.4-A is having a mean values of almost the double, 71.8 HV 1. These results let us came to the conclusion that during processing of the sample walls there was made a mistake with the wire material, so that instead EN AW-4047 the material EN AW-5356 was used for Wall Nr.4. This assumption was also backed by the results of the tensile testing where the specimens of wall Nr.4 achieved comparable results to walls Nr.5 & Nr.6. Both specimens Nr.5-A and Nr.6-A showed similar results. In case of the neglected outlier, of Nr.6-A, which was likely a hit on a pore, the mean values were almost identical with a difference of 0.8, also the standard deviation was in a close range of 2.4 (Nr.5-A) respectively 3.1 (Nr.6-A). Figure 5.2 shows a graphic of the arithmetic mean values of the hardness tests, for Nr.6 the mean value without its outlier was taken and named Nr.6*.

Comparison of the tensile tests done in this work

An effect which is visible on all stress-strain diagrams in 4.11 is the serration of curves. This behaviour - known as the Protevin-Le Chatelier effect - which occurs
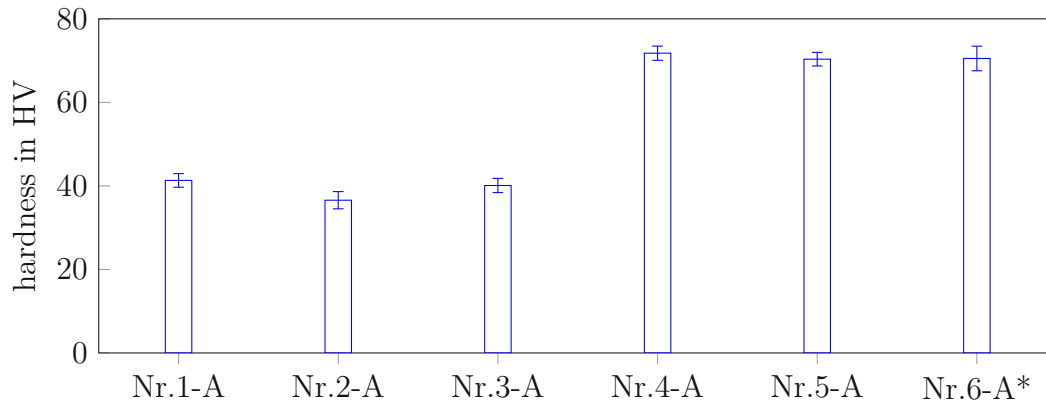
Figure 5.2: Mean value of hardness testing including the standard deviation. The * sign indicates that not all measured values were taken into account, see figure 4.6 Nr.6-A

in the plastic region of deformation [48] can induce strain hardening or also create surface weaves by deformation processes. The effect is relevant for manufacturing of thin walled metal sheet products which are manufactured by forming processes e.g., car chassis by deep drawing and might lead to unwanted optical issues. For DED this effect is of no interest since the printed parts are no concern of forming processes.

Overall, the mechanical properties differ in horizontal and vertical testing direction as mentioned in section 4.5. This behaviour arises the assumption of a deficit in the bounding between layers. A closer look on the table 4.5 reveals that some of the specimen, Nr.4 and Nr.5 show a pattern of the pores within the material which seems to have an orientation. Although there has not taken respect if the orientation of the specimens is according to the layer build up direction, it is likely that the pores form layer bands which might bring the anisotropic difference in vertical and horizontal testing direction by reducing the cross section of the vertical specimen in a higher degree then the horizontal ones. Figure 5.3 illustrates the layer band formation of the pores.

Another reason investigated by Zhao et al. [49] showed that, even if the issue of pores can be eliminated, the anisotropic character of the material still exists due concentration differences of the alloying element Mg within the deposited material. While the electric arc heats up the weld pool, a portion of Mg gets vaporized. Simultaneously, the wire gets fed to the start of the weld pool where it gets smelted and transferred to the weld pool adjacent to the solid material below. The higher Mg-enriched, smelted wire mixes with the weld pool, while it also mixes with the partially remelted previously layer. Due that a region with high and low Mg-concentration
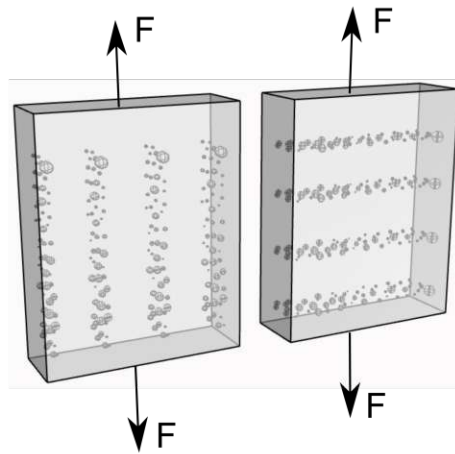
Figure 5.3: Effect of the pore band on the testing direction´s cross-section. Left: horizontal testing direction, the cross section is sectioned in multiple sections which are connected along the testing direction; Right: vertical testing direction, the cross section is sectioned in multiple sections which are interrupted by the pore band.

forms, wherein the remelted regions are high concentrated and the regions between are low concentrated with Mg. Further, the partially remelted layer is object of a faster cooling due the adjacency to solid aluminium and therefore forms smaller grains than in the regions between these remelted areas, which also gives an anisotropic character.

The loss of alloying partners is driven by the heat input of the DED energy sources (figure 2.5) which are beside joule heating characterized to work with significant higher temperatures (section 2.4) then the boiling points of all components of EN AW5356 but also of other metals.

The summarized values for the tensile tests within this work are shown in figure 5.4 where the anisotropic character between horizontal and vertical specimen can be seen.

Comparison of the tensile test results with literature for EN AW-5356

The aluminium alloy EN AW-5356 is a commonly used alloy for joint welding but also for additive manufacturing in with arc-based DED. Thanks to this there is a an abundance of scientific papers, articles and works available on the internet. We decided to compare the used plasma metal deposition process with two other commonly used arc based DED processes namely a GMAW-process [50] and the GTAW-process [51]. For the GMAW-process one of the most prominent sub-processes, the cold metal transfer (CMT) was chosen while for the GTAW-process a not closer defined process was used by the authors. It has to be mentioned that both works did observe that in the border region between layers, an increased occurrence of pores an
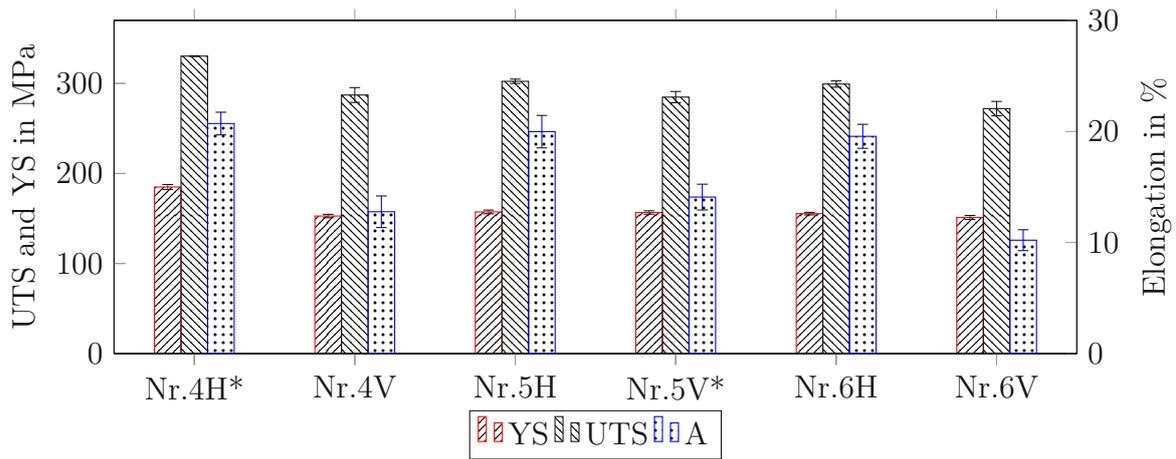
Figure 5.4: Mean values of tensile testing including the standard deviation in horizontal (H) and vertical (V) direction of the printed sample walls. The * sign indicates that not all measured values were taken into account, see table 4.7.

also microcracks were observed which also supports the assumption of porous layer bands in the border region between two layers. Therefore the results of the tensile test of the alloy EN AW-5356, the horizontal and vertical results of Nr.5H, Nr.5V*, Nr.6H and Nr.6V were combined by doing the arithmetic mean value. The graphical comparison can be seen in figure 5.5 for horizontal and vertical building direction. While the PMD process has good performance of yield strength and ultimate tensile strength in both vertical and horizontal direction the values of elongation at break are low compared to the CMT and GTAW process.
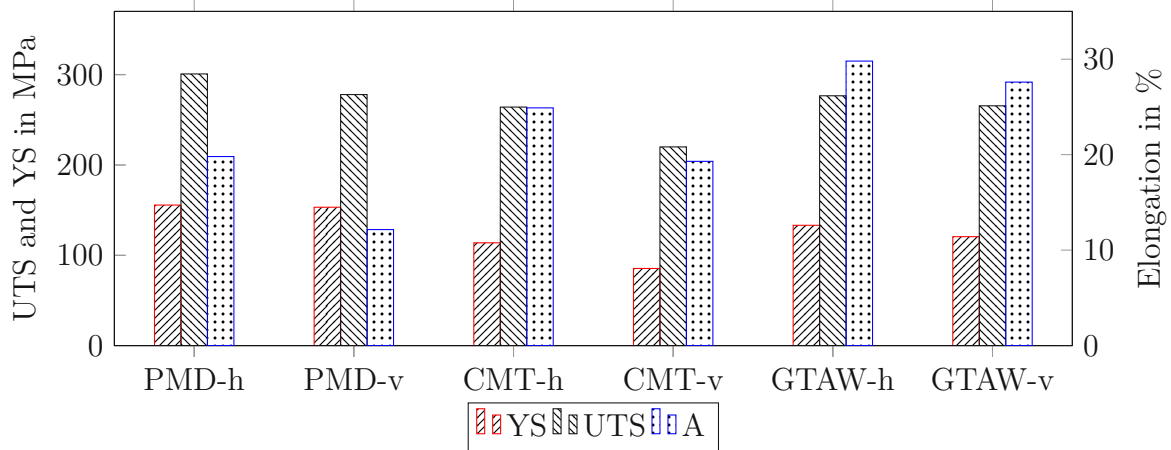
Figure 5.5: Comparison of mechanical properties (as printed) of EN AW-5356 of arc-based DED processes in horizontal (h) and vertical (v) direction.

6. Summary & conclusion

Plasma-arc based directed energy deposition (DED) of aluminium materials is often accompanied by anisotropic mechanical properties of the printed structures due pore formations in the metal matrix. This work was done to give a better understanding and overview of plasma-arc based DED of aluminium alloys (EN-AW 5356, 4043 and 4047), which is yet one of the less known additive manufacturing technologies as well as to show the influence of process parameters on the pore formation and mechanical properties.

It was demonstrated that the samples manufactured with higher energy input had in general less pores than those manufactured with lower energy input. The assumed behaviour of better mechanical properties corresponding with a lower energy input was not able to be demonstrated.

- Pores which get formed during the printing of aluminium do form a band between layers and therefore influence the anisotropic behaviour of mechanical properties but also the inhomogeneous distribution of magnesium within the printed material is responsible for the anisotropic issue. This conclusion is just relevant for EN AW-5356 thus other aluminium alloys might have different affinity to form pores.

- Linear wall structures need modified parameters for the start and stop point. As seen, the printing of aluminium is not just the definition of one parameter set and two points for start and stop. DED and in special, arc-based DED is working with weld pool sizes in the range of 3-12 millimetres in width and 0.5-2.5mm in height, the materials viscosity influences the printed surface evenness severe, especially the 4043 and 4047 alloys. Further, the tool-path has to be adopted to prevent hunch-backing or necking of the printed structure.

- EN AW-5356 seems to be better suited for use in plasma-arc based DED due a higher geometrical accuracy but also because of a better behaviour during printing which manifested in the form of a more stable arc sound and plasma arc. Additionally the pore density and size was observed to be lower in EN

AW-5356 then in the other printed materials.

- For EN AW-4043 & 4047, a lower energy input brings a higher amount of pores into the structure. By using more energy and therefore enlarging the weld pool, the dissolved gases do have more time for floating and leaving the weld pool. On the other hand, a higher energy input brings bigger weld pools and therefore issues with the geometrical accuracy of the printed structure. This behaviour was not observed at the specimen made of EN AW-5356.

References

[1] ISO/ASTM. Additive manufacturing — general principles — fundamentals and vocabulary, 2021-11. URL: https://www.iso.org/standard/74514.html.

[2] Brett E. Kelly, Indrasen Bhattacharya, Hossein Heidari, Maxim Shusteff, Christopher M. Spadaccini, and Hayden K. Taylor. Volumetric additive manufacturing via tomographic reconstruction. *Science (New York, N.Y.)*, 363(6431):1075–1079, 2019. `doi:10.1126/science.aau7114`.

[3] Crump S Scott. Apparatus and method for creating three-dimensional objects, 1992. URL: https://patentimages.storage.googleapis.com/21/01/d3/69165ba25d15e0/US5121329.pdf.

[4] Wohler Terry, Campbell Ian, Diegel Olaf, and Kowen Joseph. *Wohlers Report 2018: 3D Printing and Additive Manufacturing State of the Industry - Annual Worldwide Progress Report*. Wohlers Associates, FORT COLLINS, 2018. URL: https://wohlersassociates.com/2018report.htm.

[5] Joachim R. Daduna. Disruptive effects on logistics processes by additive manufacturing. *IFAC-PapersOnLine*, 52(13):2770–2775, 2019. `doi:10.1016/j.ifacol.2019.11.627`.

[6] Yong Huang, Ming C. Leu, Jyoti Mazumder, and Alkan Donmez. Additive manufacturing: Current state, future potential, gaps and needs, and recommendations. *Journal of Manufacturing Science and Engineering*, 137(1), 2015. URL: https://link.springer.com/article/10.1007/s11837-016-2230-5, `doi:10.1115/1.4028725`.

[7] Ralph Baker. Method of making decorative articles, 1925. URL: https://patentimages.storage.googleapis.com/83/25/a2/c6e506fcb62cf6/US1533300.pdf.

[8] Fritz Schneebeli. Method of production of workpieces by welding equipment. URL: https://patentimages.storage.googleapis.com/30/3c/0a/833df880dfb28b/US5233150.pdf.

[9] Akira Ujiie. Method and apparatus for constructing substantially cicular cross section vessel by welding. URL: https://patentimages.storage.googleapis.com/64/70/be/09e8683f7e69d0/US3558846.pdf.

[10] J. Schmidt, H. Dorner, and E. Tenckhoff. Manufacture of complex parts by shape welding. *Journal of Nuclear Materials*, 171(1):120–127, 1990. URL: https://www.sciencedirect.com/science/article/pii/002231159090356R, `doi:10.1016/0022-3115(90)90356-R`.

[11] Gerhard Posch, Fedinand Kalchgruber, Heinz Hackl, and Harald Chladil. Manufacturing of turbine blades by shape giving cmt-welding. 2014. URL: https://www.researchgate.net/publication/268778936_manufacturing-of-turbine-blades-by-shape-giving-cmt-welding.

[12] Titomic Ltd. Titomic kinetic fusion - titomic, 09.04.2022. URL: https://titomic.com/titomic-kinetic-fusion/.

[13] Impact Innovations GmbH. Additive fertigung - brennkammer, 09.04.2022. URL: https://impact-innovations.com/anwendungsbeispiele/brennkammer/.

[14] Manufactur3D. Understanding joule printing™ – a multi-metal 3d printing technology - manufactur3d, 2019. URL: https://manufactur3dmag.com/understanding-joule-printing-a-multi-metal-3d-printing-technology/.

[15] SBI GmbH. Sbi schemes and figures.

[16] Sciaky Inc. Wire-based am vs. powder-based am, 30.1.2021. URL: https://www.sciaky.com/additive-manufacturing/wire-vs-powder.

[17] Richard Görgl. Laser metal deposition: An alternative 3d printing technology.

[18] Thomas Klein, Leonhard Reiter, and Martin Schnall. Wire-arc additive manufacturing of al-zn5.5-mg-cu (ml7075): Shifting paradigms of additive manufacture-ability. *Materials Letters*, 313:131841, 2022. `doi:10.1016/j.matlet.2022.131841`.

[19] Martin Schnall. Additive manufactured piston: Email, 03.02.2021.

[20] MX3D B.V. Mx3d bridge, 30.01.2021. URL: https://mx3d.com/projects/mx3d-bridge/.

[21] Beau Jackson. Norsk titanium 3d prints world's first approved, structural, titanium components for commercial flight. *3D Printing Industry*, 10.4.2017. URL: https://3dprintingindustry.com/news/norsk-titanium-3d-prints-worlds-first-approved-structural-titanium-components-commercial-flight-110497/.

[22] Ferdinand Stempfer. Method and arrangement for building metallic objects by solid freeform fabrication, 30.03.2012. URL: https://patentimages.storage.googleapis.com/6c/8a/71/b5f299dcec6f21/US9481931.pdf.

[23] Nors Titanium. Norsk titanium | media, 09.04.2022. URL: https://www.norsktitanium.com/media#media.

[24] 3Druck.com - The Independent AM Magazine. Ramlab des hafen rotterdams präsentiert erste 3d-gedruckte schiffsschraube - update, 2017. URL: https://3druck.com/industrie/ramlab-des-hafen-rotterdams-praesentiert-erste-3d-gedruckte-schiffsschraube-1857391/.

[25] KEM Konstruktion. Ramlab fertigt schiffspropeller mithilfe eines 3d-druck-verfahrens, 2019. URL: https://kem.industrie.de/sensoren/autodesk-faro-und-ramlab-fertigen-schiffspropeller-additiv/.

[26] RAMLAB. Ramlab unveils world's first class approved 3d printed ship's propeller - ramlab, 2017. URL: https://www.ramlab.com/updates/ramlab-unveils-worlds-first-class-approved-3d-printed-ships-propeller/.

[27] Huisman Equipment B.V. 3d printing, 31.1.2021. URL: https://www.huismanequipment.com/en/about_huisman/huisman___innovation/3d_printing.

[28] 3Dnatives. Relativity space raises $140 million to become first company to launch entirely 3d printed rocket to orbit - 3dnatives, 2019. URL: https://www.3dnatives.com/en/relativity-space-140-million-3d-printed-rocket-051020194/.

[29] Erich Neubauer. Esa x-ray eye, 19.3.2021. URL: https://www.rhp-technology.com/en/our-beating-heart/esa-x-ray-eye-structure.

[30] ESA-European Space Agency. Statement of work: Trp ipc t224-004qt demonstration of an additive manufactured metallic optical bench - trp t224-004qt: Appendix 1 to ao/1-8607/16/nl/lvh.

[31] Stockhead. Titomic just launched the world's biggest 3d printer in melbourne, 2018. URL: https://stockhead.com.au/tech/titomic-just-opened-the-worlds-biggest-3d-printer-in-melbourne-heres-a-look-inside/.

[32] WAAM3D | Wire Arc Additive Manufacturing | Metal 3D printing. Robowaam — waam3d | wire arc additive manufacturing | metal 3d printing, 16.04.2022. URL: https://waam3d.com/hardware/systems.

[33] *Max-Planck-Gesellschaft Jahrbuch.* 1991. URL: https://books.google.de/books?id=17VMAQAAIAAJ.

[34] P. Kah and J. Martikainen. Influence of shielding gases in the welding of metals. *The International Journal of Advanced Manufacturing Technology*, 64(9-12):1411–1421, 2013. doi:10.1007/s00170-012-4111-6.

[35] Hans J. Fahrenwaldt and Volkmar Schuler. *Praxiswissen Schweisstechnik: Werkstoffe, Prozesse, Fertigung.* Vieweg Praxis. Vieweg+Teubner Verlag / GWV Fachverlage, Wiesbaden, Wiesbaden, 3., aktualisierte aufl. edition, 2009.

[36] Klaus-Jürgen Matthes and Werner Schneider, editors. *Schweißtechnik: Schweißen von metallischen Konstruktionswerkstoffen.* Fachbuchverlag Leipzig im Carl Hanser Verlag, München, 6., aktualisierte auflage edition, 2016.

[37] Russel Meredith. Welding torch. URL: https://patentimages.storage.googleapis.com/c2/c5/3f/8ebcd548700da1/US2274631.pdf.

[38] Robert M. Gage. Arc torch and process, 26.07.1955. URL: https://patentimages.storage.googleapis.com/55/43/e7/5523044dee961e/US2806124.pdf.

[39] R. Sarrafi and R. Kovacevic. Cathodic cleaning of oxides from aluminum surface by varibale-polarity arc: Direct real-time observation by a high-speed machine vision system shows the role of cathode spots in the cathodic cleaning of oxides and their beahvior during the cleaning process. *The Welding Journal*, (89):1–s ff., 2010. URL: http://files.aws.org/wj/supplement/wj0110-1.pdf.

[40] Linde Gas GmbH. Argon 4.6: Datasheet, 2016. URL: http://produkte.linde-gas.at/datenblatt/argon.pdf.

[41] Deutsches Institut für Normung e.V. Aluminium and aluminium alloys - chemical composition and form of wrought products: Part 1: Numerical designa-

tion system, 2005-02. URL: https://standards.iteh.ai/catalog/standards/cen/78130f9d-4ea6-44a9-9528-3380af670be7/en-573-1-2004.

[42] MIGALCO. Aluminium welding wire, 06.02.2022. URL: https://migal.co/en/products/aluminium-welding-wire.

[43] Frank Armao. Aluminum workshop: A brief overview of the other 4xxx and 5xxx filler metals, 2019. URL: https://www.thefabricator.com/thewelder/article/aluminumwelding/aluminum-workshop-a-brief-overview-of-the-other-4xxx-and-5xxx-filler-metals.

[44] TWI Ltd. - The Welding Institute. What is the difference between heat input and arc energy?, 27.05.2022. URL: https://www.twi-global.com/technical-knowledge/faqs/faq-what-is-the-difference-between-heat-input-and-arc-energy.

[45] Frank Armao. Aluminum workshop: How to recognize, minimize weld smut, 2003. URL: https://www.thefabricator.com/thewelder/article/aluminumwelding/how-to-recognize-minimize-weld-smut.

[46] R. N. Lumley. *Fundamentals of aluminium metallurgy: Production, processing and applications*. Woodhead Publishing in materials. Woodhead Pub, Oxford and Philadelphia, 2011. URL: http://search.ebscohost.com/login.aspx?direct=true&scope=site&db=nlebk&db=nlabk&AN=680662.

[47] SAFE WELDING. The dangers of welding aluminium, 2016. URL: https://safe-welding.com/welding-aluminium-dangerous-formation-of-oxides-and-ozone/.

[48] M. Abbadi, P. Hähner, and A. Zeghloul. On the characteristics of portevin–le chatelier bands in aluminum alloy 5182 under stress-controlled and strain-controlled tensile testing. *Materials Science and Engineering: A*, 337(1-2):194–201, 2002. doi:10.1016/S0921-5093(02)00036-9.

[49] DongSheng Zhao, DaiFa Long, TangRen Niu, TianFei Zhang, Xin Hu, and YuJun Liu. Effect of mg loss and microstructure on anisotropy of 5356 wire arc additive manufacturing. *Journal of Materials Engineering and Performance*, 2022. URL: https://link.springer.com/content/pdf/10.1007/s11665-022-06802-8.pdf, doi:10.1007/s11665-022-06802-8.

[50] SUN Jiaxiao, YANG Ke, WANG Qiuyu, JI Shanlin, BAO Yefeng, PAN Jie. Microstructure and mechanical properties of 5356 aluminum alloy fabricated by tig arc additive manufacturing. *Acta Metall Sin*, 57(5):665–674,

2021. URL: https://www.ams.org.cn/en/10.11900/0412.1961.2020.00266, `doi: 10.11900/0412.1961.2020.00266`.

[51] Jiankun Wang, Qingkai Shen, Xiangdong Kong, and Xizhang Chen. Arc additively manufactured 5356 aluminum alloy with cable-type welding wire: Microstructure and mechanical properties. *Journal of Materials Engineering and Performance*, 30(10):7472–7478, 2021. URL: https://link.springer.com/article/10.1007/s11665-021-05905-y, `doi:10.1007/s11665-021-05905-y`.